

Coordination Pattern of Two Imidazole-Chalcone Hybrid Ligands and Reactivity Analysis of Their Transition Metal (II) Complexes by Density Functional Theory

Julius Numbonui Ghogomu^{1,2*} and Fitzgerald Kogge Bine¹

¹University of Dschang, Research Unit of Noxious Chemistry and Environmental Engineering, Department of Chemistry, Faculty of Science, P.O. Box 67, Dschang, Cameroon

²The University of Bamenda, Department of Chemistry, Faculty of Science, P.O. Box 39, Bambili-Bamenda, Cameroon

***Corresponding Author:** Julius Numbonui Ghogomu, University of Dschang, Research Unit of Noxious Chemistry and Environmental Engineering, Department of Chemistry, Faculty of Science, P.O. Box 67, Dschang, Cameroon.

Received: March 26, 2020; **Published:** April 06, 2020

Abstract

A DFT study of the coordination behavior of two imidazole-based chalcone ligands: 2-[1-(3-(1H-imidazol-1-yl)propylimino)-3-(phenylallyl)]phenol and 2-[1-(3-(1H-imidazol-1-yl)propylimino)-3-4-nitrophenylallyl]phenol (herein dubbed HL1 and HL2 respectively) toward Co^{2+} , Cu^{2+} , Ni^{2+} and Zn^{2+} ions, and reactivity analysis of the resulting complexes is reported. The dispersion-corrected DFT (DFT-D3), conceptual DFT, quantum theory of atoms-in-molecules (QTAIM), molecular electrostatic potential (MEP) and the non-covalent interaction (NCI) index approaches were used. Both HL1 and HL2 are found to utilize variable imidazole ring-based donor sites to coordinate with metal ions, contrary to some earlier studies asserting that these species only act as tridentate ligands bearing a unique set of donor atoms toward metal (II) ions.

Interestingly, the Ni (II) complexes of both ligands and the Zn (II) complex of HL1 turned out to be organometallic species. Diverse non-covalent intramolecular interactions were elucidated in all compounds, playing key roles in molecular integrity. Our results also showed that HL2 and its complexes are more reactive than their HL1 counterparts, owing to their higher electrophilicity indices. Moreover, whereas the metal ion center (except the Zn(II) ion) in all complexes studied are liable to attack by nucleophiles, the carbon and oxygen atoms of the phenolic moiety alongside the chloride ligands, are most favorable sites for electrophilic attack.

Keywords: DFT, QTAIM, NCI index, Reactivity Analysis; Imidazole-chalcone hybrid

Abbreviations: HL1: 2-[1-(3-(1H-imidazol-1-yl) propylimino)-3- (phenylallyl)] phenol HL2: 2-[1-(3-(1H-imidazol-1-yl) propylimino)-3-4-nitrophenylallyl] phenol; HL1-M and HL2-M: where M= Co(II), Cu(II), Ni(II) & Zn(II), are the corresponding transition metal complexes of HL1 and HL2; GGA: Generalized gradient approximation; DFT: Density functional theory; DFT-D3: Dispersion-corrected DFT; CDFT: Conceptual DFT; QTAIM: Quantum theory of atoms-in-molecules; MEP: Molecular electrostatic potential; NCI: Non-covalent interaction; LRDs: Local reactivity descriptors; GRDs: Global reactivity descriptors; RDG: Reduced density gradient; QSAR: Quantitative structure activity relationships; BJ: Becke-Johnson; UKS: Unrestricted Kohn-Sham; RKS: Restricted Kohn-Sham; RI: Resolution of the identity approximation; COSX : chain-of-spheres approximation

Citation: Julius Numbonui Ghogomu and Fitzgerald Kogge Bine. (2020). Coordination Pattern of Two Imidazole-Chalcone Hybrid Ligands and Reactivity Analysis of Their Transition Metal (II) Complexes by Density Functional Theory. *Archives of Chemistry and Chemical Engineering* 2(1).

Introduction

Drug resistance remains a major challenge to public health today and proactive measures such as the search for novel and more potent drugs are necessary solutions. Chalcones for instance are natural products containing an α,β -unsaturated ketone moiety (pharmacophore) that is responsible for their biological activities. They are ubiquitous in edible plant species such as *Angelica*, *Glycyrrhiza*, *Humulus* and *Scutellaria*, and are widely used as traditional folk remedies for cancer, fungi, malaria, and HIV [1-3]. Chalcones are commonly synthesized by the Claisen-Schmidt condensation reaction between acetophenone and benzaldehyde (or their derivatives), in the presence of aqueous alkali media [5].

Clinical studies have elucidated their excellent bioavailability and tolerance in the human body especially when coordinated with metal ions [3,6]. Although chalcones generally exist in both the E and Z forms [3], the E form is predominant in chalcones bearing a hydroxyl group at the 2'-position (C25 in those currently investigated, see Figure 1) due to inhibition of E to Z photo-isomerisation. Additionally, the E isomer is thermodynamically more stable than the Z isomer [4]. The bioactivities of chalcones have been found to be enhanced by incorporation of some supplementary pharmacophores such as "azole" moieties [7,8]. Chalcone-imidazole hybrids have electron rich centers on the imidazole ring which facilitate binding to a variety of enzymes and receptors in biological systems through diverse weak interactions, thereby conferring on them a broad spectrum of bioactivities [9]. The imidazole ring with its multiple binding sites is also capable of coordinating with a variety of metal ions, as well as interacting with other organic molecules via non-covalent bonds. This leads to the formation of supramolecular drugs, which are less susceptible to drug resistance [10,11]. Accordingly, one of the main objectives of this study has been to provide more insights into the binding modes of two imidazole-based chalcones, in view of designing much more effective drugs for the treatment of the aforementioned pandemics.

From literature survey, tridentate chelates of Co(II), Ni(II), Cu(II) and Zn(II) with the imidazole-based chalcone ligands: 2-[1-(3-(1H-imidazol-1-yl)propylimino)-3-(phenylallyl)]phenol (HL1), 2-[1-(3-(1H-imidazol-1-yl)propylimino)-3-4-nitrophenylallyl]phenol (HL2) are reported to exhibit interesting strong to moderate antifungal activities on *Candida albicans* [12]. Despite these and other interesting biological activities of HL1 and HL2 alongside their metal complexes, little work has been carried out on their mechanism of

action. In order to facilitate the elucidation of these mechanisms, some structural and reactivity analyses have been performed herein. On the basis of an experimental study on HL1 and HL2 [12] and a follow-up theoretical investigation [13], it has been observed that only the azomethine nitrogen (N17) of the imidazole moiety, the phenolic oxygen (O26) and the iminic nitrogen (N11) of the chalcone moiety of HL1 and HL2 act as electron donors to metal ions, as shown in Figure 1.

However, a contrary opinion that other atoms of the imidazole ring may also serve as donor atoms owing to the availability of multiple binding sites, has been reported elsewhere [10,11] in other imidazole-based compounds. To investigate whether or not these multiple binding sites exist in the chalcones currently studied, further structural investigations on these complexes are warranted. Moreover, as potential antifungal drugs [12], in-depth chemical reactivity studies on HL1 and HL2 and their metal complexes need to be carried out. Although the antimicrobial activities of these molecules were investigated in a previous study [13] from the viewpoint of frontier molecular orbital analysis alone, further insights from conceptual density functional theory (DFT)-based reactivity descriptors and molecular electrostatic potential maps are indispensable. Given that the understanding and tailoring of weak molecular interactions is crucial to the design of new molecules and materials with desired properties [14], the non-covalent interactions in the compounds investigated are also of interest in this work. It should be recalled that structural, conformational and electronic properties contribute to a perfect mastery of a drug candidate in view of optimizing its design [15].

To address the aforementioned concerns, a comprehensive DFT study of the coordination pattern of HL1 and HL2 toward some transition metal (II) ions, and the chemical reactivity of the resulting complexes have been undertaken. The DFT method has been chosen here for reasons of its good compromise between computational accuracy and cost [16,17]. Also, conceptual-DFT, the quantum theory of atoms-in-molecules (QTAIM), the non-covalent interaction (NCI) index and molecular electrostatic potential (MEP) maps analyses tools were exploited accordingly. The molecular structures, along with the atom numbering schemes of all investigated species, are presented in Figure 1.

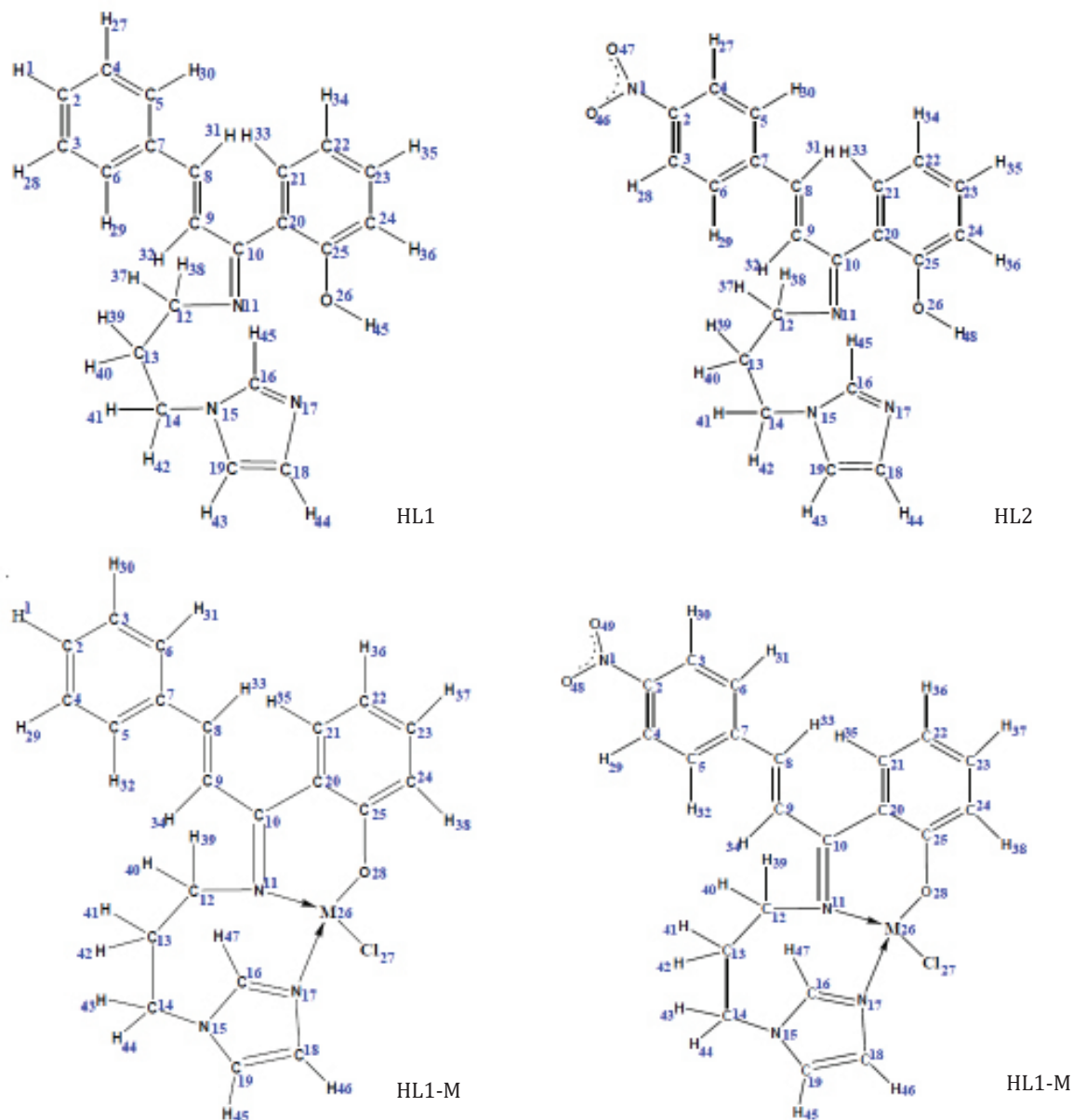


Figure 1: Input structures and numeration of studied ligands and complexes with $M = \text{Co(II)}, \text{Cu(II)}, \text{Ni(II)} \text{ \& } \text{Zn(II)}$.

Computational details

Theoretical calculations were carried out via the ORCA quantum chemical package [18] (versions 4.0.1 and 3.0.3). ORCA 3.0.3 was only used in the single point calculations aimed at generating input files for MEP analysis. Other input files were prepared with the Avogadro 1.1.1 visualization software [19]. Geometry optimization and frequency calculations were performed using the DFT method in conjunction with the def2-TZVP Ahlrichs basis set in association with the corresponding auxiliary (coulomb-fitting)

basis set [20,21]. The GGA functional BP86 [22, 23] was used for geometry optimizations and frequency calculations because it predicts excellent geometries and vibrational frequencies [24,16]. The BP86-D3 optimized structures were further optimized and vibrational frequencies computed using the B97-3c composite electronic structure approach [25]. The choice of the B97-3c approach was motivated by the fact it is a well-tested low-cost method that is recommended for geometry optimization, and is found to yield excellent molecular geometries of metal-organic and large systems

Citation: Julius Numbonui Ghogomu and Fitzgerald Kogge Bine. (2020). Coordination Pattern of Two Imidazole-Chalcone Hybrid Ligands and Reactivity Analysis of Their Transition Metal (II) Complexes by Density Functional Theory. *Archives of Chemistry and Chemical Engineering* 2(1).

[25]. To speed-up the geometry optimization and frequency calculations, but with marginal loss in accuracy, the resolution-of-the-identity (RI-J) approximation [26] was used in conjunction with appropriate auxiliary basis sets. Furthermore, long-range dispersion interactions were incorporated via the Grimme's atom-pairwise dispersion correction using the Becke-Johnson damping scheme (D3BJ) [27, 28], since pure exchange-correlation functionals fail to properly account for such interactions.

The geometries of the Co (II) complexes at the doublet and quartet spin states, as well as those of the Ni (II) complexes at the singlet- and triplet-states, were optimized in a bid to determine the most stable spin state in each case that corresponds to the most stable geometry. The geometries of the Cu (II) and Zn (II) complexes were optimized at their lowest spin states i.e. doublet and singlet respectively, since higher spin states are not possible in these cases. It must be pointed out that the doublet-, triplet- and quartet-state complexes were optimized using the Unrestricted Kohn-Sham (UKS) formalism, whereas the singlet-state complexes were optimized using the Restricted Kohn-Sham (RKS) formalism. No constraints on symmetry, bond lengths, bond angles or dihedral angles were applied in the geometry optimization calculations. In order to be sure that we obtained reliable and stable structures (minima on the PES), vibrational frequencies were calculated for all optimized structures and their analyses revealed no imaginary frequencies.

In the implementation of conceptual DFT for the evaluation of ionization energies and electron affinities, the hybrid Meta-GGA functionals, M06 for the complexes and M06-2X for the organic molecules (HL1 and HL2) as recommended in [29], were used for single point energy calculations on the BP86-optimized geometries. The Minnesota functionals (M06 and M06-2X) were chosen here because they incorporate an inbuilt dispersion correction, and also perform well for energy calculations [29]. These functionals were employed along with the ma-def2-TZVP all-electron basis set. To speed-up the calculations with the hybrid functionals, the RI-J approximation was used in combination with the chain-of-spheres (COSX) approximation, giving rise to the RIJCOSX approximation [30]. Throughout the ORCA calculations, numerical quadrature grids of at least 5 were used.

Results and Discussion

Spin state stability analysis

In order to find the most stable spin state corresponding to the lowest energy geometries, the electronic energies of the Co(II) complexes optimized at doublet and quartet states, and the Ni(II) complexes optimized at singlet and triplet states, are compared in Table 1. It is clear from this table that the higher spin states of both the Co (II) and Ni (II) complexes are more stable by virtue of their lower electronic energies compared to the lower spin states [13]. Thereof, the quartet and triplet states of Co (II) and Ni (II) complexes are respectively considered for further studies.

Complex	BP86-D3BJ/Def2-TZVP				B97-3c			
	Singlet	Doublet	Triplet	Quartet	Singlet	Doublet	Triplet	Quartet
HL1-Ni	-3021.05	–	-3021.18	–	-3019.92	–	-3020.09	–
HL1-Co	–	-2895.48	–	-2895.61	–	-2894.29	–	-2894.47
HL2-Ni	-3225.67	–	-3225.80	–	-3224.34	–	-3224.52	–
HL2-Co	–	-3100.10	–	-3100.24	–	-3098.71	–	-3100.24

Table 1: Energies (in Hartrees) of HL1-Mand HL2-M, (where M= Co (II), Ni (II) complexes optimized at RI-BP86/def2-TZVP and B97-3c levels of theory.

Structural and geometric analysis

In this study, structural analyses have been performed based on the gas phase optimized structures. The initial guesses for the geometry optimizations were constructed based on the geometries suggested in a previous investigation from the literature [12]. According to the authors, the N17 nitrogen atom of the imidazole ring

can act as a donor atom to a central metal during complex formation. In order to complement these findings theoretically, geometry optimizations were performed as described earlier and selected geometric parameters (bond lengths, bond angles and dihedral or torsional angles) are listed in Tables 2a and 2b. In addition, the optimized geometries of the complexes are shown in Figure 2, as visualized using the Chemcraft 1.8 visualization software [31].

A detailed inspection of Tables 2a and 2b reveals a good agreement between the geometrical parameters computed at the RI-BP86-D3 (BJ)/def2-TZVP and B97-3c levels of theory. Based on this observation, it can be concluded that similar optimized structures are

obtained by both methods. This is expected since both dispersion-corrected BP86 functional and the B97-3c composite method yield excellent geometries [16,24,25]. However, much attention is focused herein on the results obtained at the RI-BP86-D3 (BJ)/def2-TZVP.

Geometric parameters	RI-BP86-D3(BJ)/def2-TZVP				B97-3c			
Bond Lengths (Å)	HL1-Co	HL1-Ni	HL1-Cu	HL1-Zn	HL1-Co	HL1-Ni	HL1-Cu	HL1-Zn
M-N ₁₁	1.953	1.931	1.924	1.986	1.965	1.937	1.946	1.995
M-O ₂₈	1.872	1.855	1.847	1.891	1.876	1.862	1.866	1.899
M-Cl ₂₇	2.192	2.196	2.144	2.180	2.214	2.219	2.173	2.198
M-C ₁₆	–	2.270	–	–	–	2.281	–	–
M-C ₁₉	–	–	–	2.616	–	–	–	2.637
M-N ₁₇	2.186	–	–	–	2.205	–	–	–
Bond Angles (°)								
O ₂₈ -M-N ₁₁	96.6	94.7	95.5	98.4	96.1	94.5	94.7	98.2
N ₁₁ -M-Cl ₂₇	108.6	112.4	117.9	117.5	109.8	113.1	119.6	118.4
Cl ₂₇ -M-C ₁₆	–	99.4	–	–	–	99.5	–	–
Cl ₂₇ -M-N ₁₇	105.3	–	–	–	106.0	–	–	–
O ₂₈ -M-N ₁₇	109.6	–	–	–	109.7	–	–	–
C ₁₉ -M-O ₂₈	–	–	–	115.1	–	–	–	117.4
Dihedral Angles (°)								
O ₂₈ -M-Cl ₂₇ -N ₁₁	111.2	128.4	171.1	140.2	111.5	128.2	166.0	137.7
O ₂₈ -M-Cl ₂₇ -N ₁₇	-126.2	–	–	–	-126.9	–	–	–
O ₂₈ -M-Cl ₂₇ -C ₁₆	–	-138.1	–	–	–	-137.5	–	–
Cl ₂₇ -M-N ₁₇ -N ₁₁	118.9	–	–	–	119.9	–	–	–
Cl ₂₇ -M-C ₁₉ -N ₁₁	–	–	–	117.5	–	–	–	118.4
Cl ₂₇ -M-C ₁₆ -N ₁₁	–	112.7	–	–	–	113.4	–	–

Table 2a: Some selected geometric parameters in gas phase of studied complexes at RI-BP86-D3 (BJ)/def2-TZVP, RI-TPSS-D3(BJ)/def2-TZVP & B97-3c levels of theory.

Although it is proposed in [12] and [13] that the N17 nitrogen is the unique donor atom of the imidazole ring in HL1 and HL2, our results as can be seen from Tables (2a and 2b) and Figure 2 demonstrate the possibility of other imidazole ring atoms acting as donors as well. This phenomenon is quite noticeable in the HL1-Ni, HL2-Ni and HL1-Zn complexes, wherein the carbon atoms C₁₆ and C₁₉ act as donor atoms instead of N₁₇. In contrast to the findings in [12] and [13], our results have shown that HL1-Ni, HL2-Ni and HL1-Zn are essentially organometallic in nature. However, the tetragonal geometry around the central metal is maintained as predicted by kalanithi and co-workers [12]. Surprisingly, in the

HL1-Cu, HL2-Cu and the HL2-Zn complexes, the imidazole moiety fails to bind to the central metal ion via any of its donor atoms, resulting in distorted trigonal planar geometries around the central metal ions, which is somewhat consistent with the distorted planar geometries elucidated experimentally for the Cu (II) complexes [12]. It has been observed that apart from the Zn-C bond, the lengths of the metal-ligand (M-L) bonds: M-N, M-O, M-Cl and other M-C fall within the typical range 1.797–2.258 Å [32, 33]. It is necessary to point out that the organometallic bond distances (2.25–2.63 Å) as computed at both RI-BP86-D3(BJ)/def2-TZVP and B97-3c levels, are relatively longer than the other M-L distances (1.847–2.219

Å), suggesting that the organometallic bonds may be weaker than the rest of the M-L bonds, as expected.

Geometric parameters	RI-BP86-D3(BJ)/def2-TZVP				B97-3c			
Bond Lengths (Å)	HL2-Co	HL2-Ni	HL2-Cu	HL2-Zn	HL2-Co	HL2-Ni	HL2-Cu	HL2-Zn
M-N ₁₁	1.955	1.930	1.925	1.997	1.955	1.936	1.945	2.003
M-O ₂₈	1.882	1.857	1.847	1.886	1.884	1.864	1.864	1.894
M-Cl ₂₇	2.185	2.195	2.140	2.155	2.185	2.218	2.170	2.172
M-C ₁₆	–	2.251	–	–	–	2.262	–	–
M-N ₁₇	2.165	–	–	–	2.165	–	–	–
Bond Angles (°)								
O ₂₈ -M-N ₁₁	96.3	94.7	95.4	97.4	96.3	94.6	94.9	97.3
N ₁₁ -M-Cl ₂₇	109.6	111.8	118.1	117.3	109.6	112.5	119.2	118.0
Cl ₂₇ -M-C ₁₆	–	99.6	–	–	–	99.8	–	–
Cl ₂₇ -M-N ₁₇	105.4	–	–	–	105.4	–	–	–
O ₂₈ -M-N ₁₇	104.6	–	–	–	104.6	–	–	–
Dihedral Angles (°)								
O ₂₈ -M-Cl ₂₇ -N ₁₁	113.5	128.0	172.4	147.7	113.5	127.8	166.6	142.2
O ₂₈ -M-Cl ₂₇ -N ₁₇	-121.3	–	–	–	-121.3	–	–	–
O ₂₈ -M-Cl ₂₇ -C ₁₆	–	-137.8	–	–	–	-137.2	–	–
Cl ₂₇ -M-N ₁₇ -N ₁₁	121.3	–	–	–	121.3	–	–	–
Cl ₂₇ -M-C ₁₆ -N ₁₁	–	112.2	–	–	–	113.0	–	–

Table 2b: Some selected geometric parameters in gas phase of studied complexes at RI-BP86-D3 (BJ)/def2-TZVP, RI-TPSS-D3 (BJ)/def2-TZVP & B97-3c levels of theory.

The calculated bond angles around the central metal ions in the Co(II), Ni(II) and Zn(II) complexes differ slightly from the standard 109.5° (in perfectly tetrahedral complexes), thus revealing distorted tetrahedral geometries around these ions in their respective complexes currently investigated. On the part of the HL1-Cu, HL2-Cu and HL2-Zn complexes, distorted trigonal planar geometries have been observed, in which the ligands HL1 and HL2 are bidentate. In HL1-Cu, the extent of the trigonal planar geometry distortion from perfect planarity is minimal, as demonstrated by the dihedral angle O₂₈-M-Cl₂₇-N₁₁ (171.1°), which is ~8.9° off 180°. A similarly observation can be made in the case of HL2-Cu. However, in the case of HL2-Zn, the torsional angle O₂₈-M-Cl₂₇-N₁₁ (147.7°) deviates significantly from the corresponding value in a perfect trigonal planar geometry by 39.8°, indicating that HL2-Zn is highly distorted relative to HL1-Cu and HL2-Cu.

Local nucleophilicity at the imidazole ring of HL1 and HL2 ligands

To gain a deeper understanding of the possible coordination sites of the imidazole moiety in the investigated ligands, the local nucleophilicity indices and the Fukui function values of all atoms in the five-member ring have been explored. This in-depth analysis has been performed in a bid to confirm the variable binding mode ability of the imidazole moiety, as earlier predicted by the gas phase optimized structures of the complexes of HL1 and HL2, and as suggested in [10] and [11]. This behavior has been explained from the viewpoint of the local reactivity (nucleophilicity) of the atoms comprising the imidazole moiety (N₁₅, C₁₆, N₁₇, C₁₈ and C₁₉), which has been predicted from conceptual DFT-based reactivity indices and molecular electrostatic (MEP) potential maps.

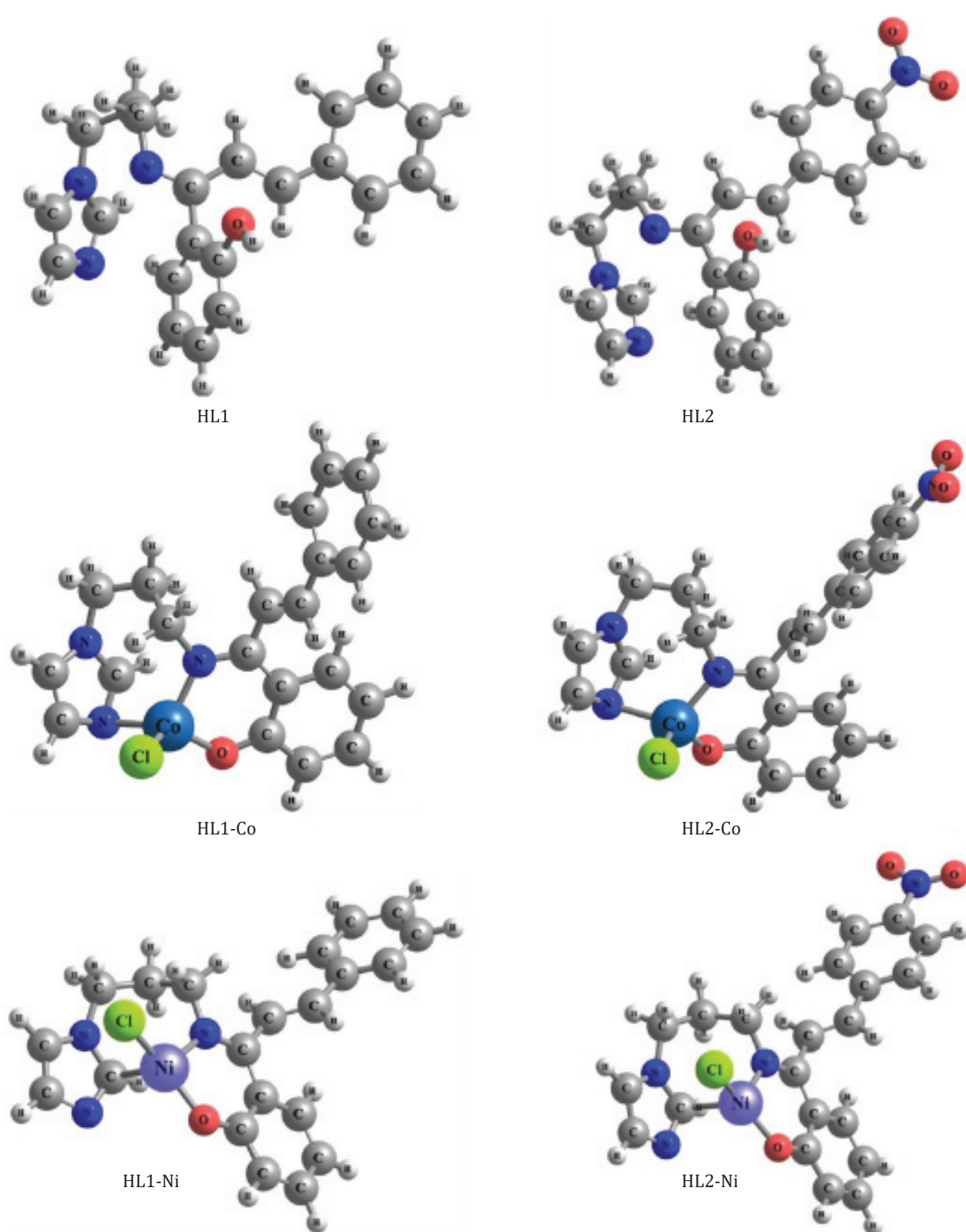


Figure 2: Optimized structures of studied HL1 compounds in gas phase at the RI-BP86-D3(BJ)/def2-TZVP level of theory

Citation: Julius Numbonui Ghogomu and Fritzgerald Kogge Bine. (2020). Coordination Pattern of Two Imidazole-Chalcone Hybrid Ligands and Reactivity Analysis of Their Transition Metal (II) Complexes by Density Functional Theory. *Archives of Chemistry and Chemical Engineering* 2(1).

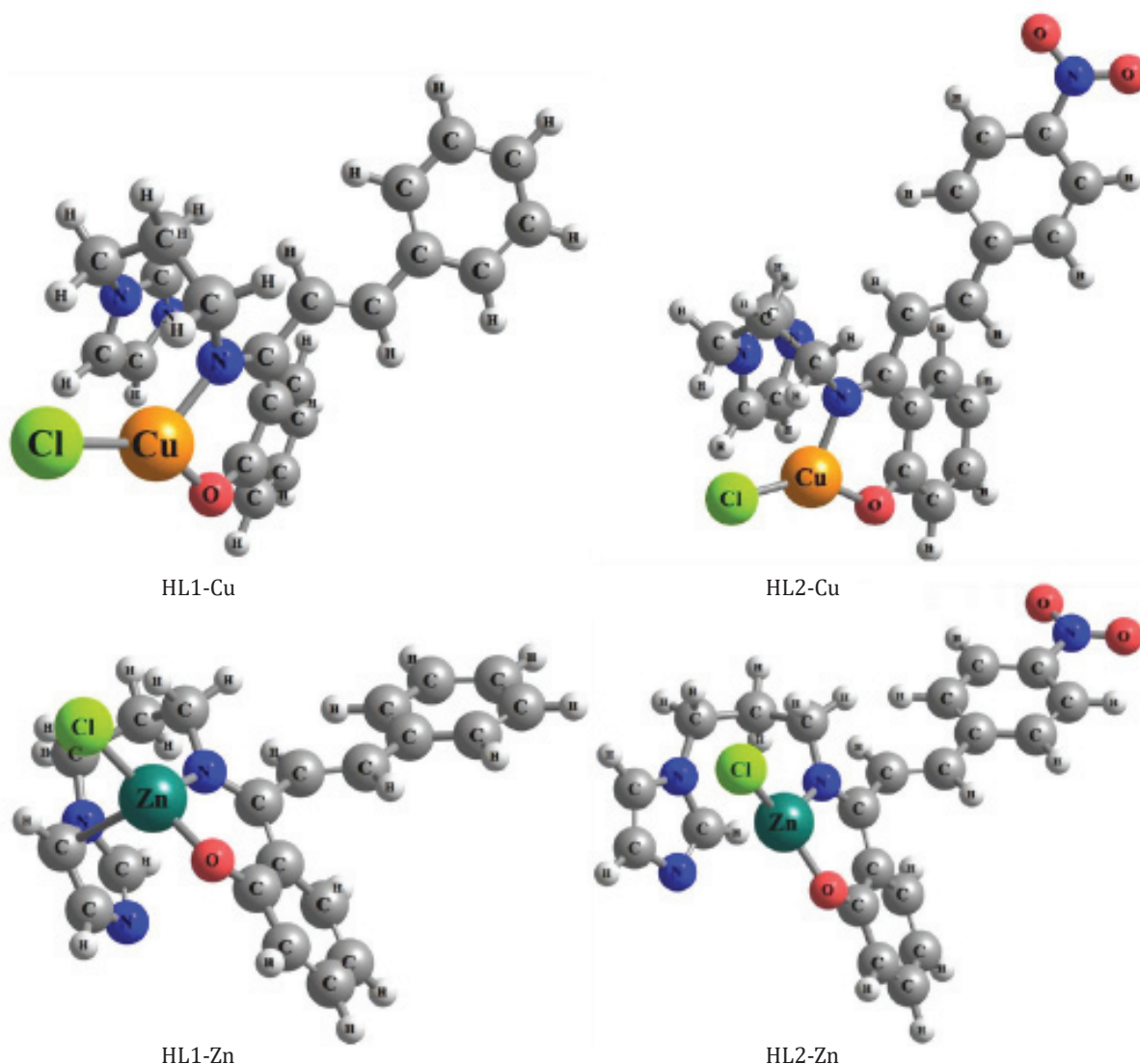


Figure 2: Continued

In the realm of conceptual DFT (CDFT), local reactivity descriptors (LRD) have been proposed to describe the selectivity or reactivity of atom sites in a molecule [34]. The LRDs used in this work include: the Fukui functions for electrophilic attack (f_k^-) and nucleophilic attack (f_k^+) on the k th atom in each molecule studied, the dual descriptor ($\Delta f(r)$) and the local nucleophilicity index (LNI). These LRDs have been calculated from single point energies computed at RIJCOSX-M06-2X/def2-TZVP//RI-BP86-D3 (BJ)/def2-TZVP level of theory. The Fukui function ($f(r)$) is defined as the first derivative of the electronic density $\rho(r)$ of a system with respect to the number of electrons N at a constant external potential $v(r)$ [34].

$$f(r) = \left[\frac{\partial \rho(r)}{\partial N} \right]_{v(r)} \quad (1)$$

In Equation (1), the electrophilic and nucleophilic condensed Fukui function by the finite difference approximations from Hirshfeld population analysis, can be defined according to Equations (2) and (3) respectively, as proposed by Yang and Motier [35].

$$f_k^- = q_k(N) - q_k(N-1) \quad (2)$$

$$f_k^+ = q_k(N+1) - q_k(N) \quad (3)$$

Where $q_k(N)$, $q_k(N-1)$ and $q_k(N+1)$ are, respectively, the electronic population of the k th atom in the neutral, cationic and anionic species with identical geometries so that the external potential is maintained constant. The higher the f_k^- value for the k th atom, the more favourable it is for electrophilic attack (acting as a nucleophile). The dual descriptor Δf_k is closely related to the Fukui function, and is given by Equations (4):

$$\Delta f_k = f_k^+ - f_k^- = 2q_k(N) - q_k(N+1) - q_k(N-1) \quad (4)$$

In general, when $\Delta f_k > 0$ the site is favorable for nucleophilic attack, whereas when $\Delta f_k < 0$ the site is favorable for electrophilic attack [36].

Nucleophilicity indices have been computed in this work according to the nucleophilicity model proposed by Pérez and coworkers [37]. On the basis of this model, the global nucleophilicity index, N , can be expressed as the sum of local nucleophilicities condensed to all atoms of a given molecule, as in the following equation:

$$N = \sum_k N_k \quad (5)$$

From Equation (5), the local nucleophilicity index condensed to an atom k th, N_k , is related to the nucleophilic Fukui function, f_k^- , via Equation (6).

$$N_k = N f_k^- \quad (6)$$

It should be noted that in calculating the value of N used in equation (6), we made use of the empirical (relative) N index proposed by Domingo and co-workers [38] for closed-shell organic molecules based on the HOMO energies (E_{HOMO}) obtained within the Kohn-Sham scheme in gas phase, and defined as in Equation (7):

$$N = E_{\text{HOMO}}(\text{Nucleophile}) - E_{\text{HOMO}}(\text{TCE}) \quad (7)$$

As can be seen from Equation (7), N is computed as the difference between the E_{HOMO} of the molecule of interest (Nucleophile) and tetracyanoethylene (TCE), the latter being the most electrophilic (or least nucleophilic) neutral species for a large series of molecules [39].

The calculated values of the Fukui functions (f -and f^+), local nucleophilicity (N_k) and the dual descriptor (Δf) for HL1 and HL2 are listed Table 3, whereas those of the global nucleophilicity index (N) are listed in Table S1. From the Δf values in Table 3, it is clear that

all atoms of the five-membered imidazole ring are prone to electrophilic attack or can easily act as nucleophiles. This implies that these atoms can act as potential electron donors to a central metal atom/ion, leading to the formation of coordinate bonds. Surprisingly, from the trend shown by the Δf_k and N_k values for HL1 ($N_{15} < N_{17} < C_{16} < C_{19} < C_{18}$) and HL2 ($N_{15} < N_{17} < C_{16} < C_{18} < C_{19}$), it is evident that the carbon atoms the imidazole ring are even more susceptible to coordinate with central metal atoms/ions than the nitrogen atoms. This observation is contradictory to earlier studies [12, 13], which show that only one of the nitrogen atoms (N17) is the unique donor of the imidazole moiety. This also justifies the formation of organometallic compounds of HL1 and HL2 with some metal ions, as earlier observed in the optimized structures investigated herein. It must be pointed out that carbon atoms of the imidazole moiety are more sterically hindered than N17 since they each bear a hydrogen atom, which somewhat reduces their propensity to coordinate to the central metal.

Compound	Atomic sites	f^-	f^+	Δf	N_k
HL1	N ₁₅	0.01109	-0.0044	-0.0155	0.03693
	C ₁₆	0.03725	0.00069	-0.0366	0.12406
	N ₁₇	0.02655	0.01249	-0.0141	0.08844
	C ₁₈	0.04656	0.00961	-0.037	0.1551
	C ₁₉	0.03987	0.00089	-0.039	0.1328
HL2	N ₁₅	0.02481	-0.0032	-0.028	0.07771
	C ₁₆	0.07861	-0.0002	-0.0788	0.2462
	N ₁₇	0.04317	0.00889	-0.0343	0.13522
	C ₁₈	0.08705	0.00731	-0.0797	0.27264
	C ₁₉	0.09006	0.00119	-0.0889	0.28206

Table 3: Local Nucleophilicity (N_k) and dual descriptors at the imidazole moiety of HL1 and HL2.

In order to supplement the results obtained from the local reactivity descriptors (Δf_k and N_k), molecular electronic potential (MEP) maps of HL1 and HL2 have been computed in gas phase at RIJCOSX-M06-2X/def2-TZVP level of theory, based on their gas phase optimized structures. The generation and visualization of the maps have been aided by the Molekel 4.3 graphical user interface. The calculations of the MEP surfaces in this study are based on the theory previously highlighted in [40]. As can be observed from Figure 3, the electron density around the imidazole ring in each ligand is high, and is well delocalized over the N₁₇, C₁₆, C₁₈ and C₁₉, especially

in HL2. This observation corroborates the fact that the C₁₆, C₁₈ and C₁₉ atoms also have the ability to act as donor atoms to the central metal atom besides N₁₇.

QTAIM analysis of compounds under study

To provide detailed insights into the nature of the metal-ligand (M-L) interactions alongside other intramolecular interactions in the molecules under study, such as hydrogen bonds (HBs), van der Waal interactions and H···H interactions, with particular attention focused on the metal-imidazole moiety interactions, Bader's QTAIM analysis has been performed via the Multiwfn 3.6(dev) software [41]. It is worthy of note that these interactions help maintain the shapes and contribute to the stability of these compounds, as well as determine their functionality in biological systems [42]. In topology analysis, the real space function known as eta index (η), given by $\eta = |\lambda_1(r)|/(\lambda_3(r))$ where λ_1 and λ_3 are the lowest and the highest eigen values of hessian matrix of the electron density, ρ , respectively, has been argued to have values at bond critical point less than unity for closed shell interactions such ionic, van der Waals, H-bonding, and dihydrogen-bonding interactions and increases with increasing covalent character [43]. In the present study, topological analyses of other real space functions such as the electron density and its laplacian have been performed at bond critical points. Large $\rho(r)$ values and $\nabla^2 \rho(r) < 0$ indicate polar and non-polar covalent bonding interactions, whereas small $\rho(r)$ values and $\nabla^2 \rho(r) > 0$ indicate closed-shell interactions [42]. Generally, $\rho(r)$ is greater than 0.20 a.u. for covalent bonding interactions and less than 0.10 a.u. for closed-shell interactions [42]. The values of $\nabla^2 \rho(r)$ and $-G(r)/V(r)$ were also used to characterize the bonding interactions in the compounds studied based on the literature highlighted in [40]. In the context of QTAIM analysis, Popelier [44] developed some useful criteria for characterizing hydrogen bonds (HBs), which have been exploited in this work. According to Popelier, the formation of an HB depends on the electron density and it's Laplacian at the BCP, which should lie in the range of 0.002–0.040 a.u. and 0.024–0.139 a.u., respectively.

Espinosa [45] formulated an equation of the form $E_{\text{int}} = 0.5 V(r)$, which is useful for estimating weak interatomic interaction energies, particularly HB energies. In this equation, $V(r)$ is the potential energy density. The non-covalent interactions and their real space functions computed in this work at RI-BP86-D3 (BJ)/def2-TZVP level are presented in Table 4, along with their interaction energies. The corresponding molecular graphs are shown in Figure S1.

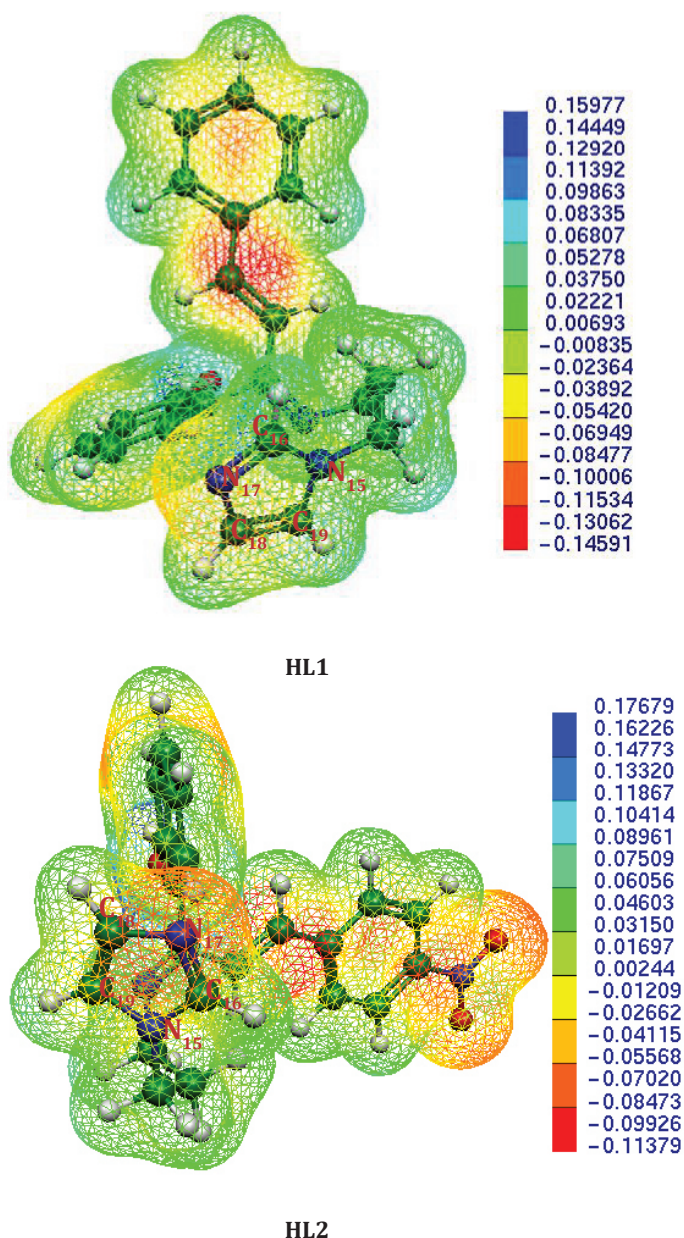


Figure 3: MEP maps of ligands showing electron density distribution over the imidazole moieties

Bonding Interaction	$\rho(r)$	$\nabla^2 \rho(r)$	$G(r)$	$v(r)$	$-G/v$	eta index	E_{int}
HL1-Co							
Co ₂₆ -O ₂₈	0.1093	0.5835	0.1729	-0.1998	0.8650	0.1765	-62.7034
Co ₂₆ -N ₁₁	0.1007	0.4313	0.1361	-0.1644	0.8280	0.1797	-51.5672
Co ₂₆ -Cl ₂₇	0.0858	0.2600	0.0910	-0.1170	0.7778	0.2094	-36.7185
Co ₂₆ -C ₁₆	0.0559	0.2021	0.0599	-0.0692	0.8650	0.1832	-21.7105
H ₃₅ ...C ₉	0.0166	0.0546	0.0121	-0.0106	1.1468	0.1780	-3.3116
H ₃₄ ...H ₃₁	0.0106	0.0401	0.0084	-0.0067	1.2478	0.1872	-2.1019
HL1-Cu							
Cu ₂₆ -O ₂₈	0.1140	0.5422	0.1713	-0.2071	0.8274	0.1954	-64.962
Cu ₂₆ -N ₁₁	0.1070	0.3893	0.1346	-0.1719	0.7832	0.2163	-53.925
Cu ₂₆ -Cl ₂₇	0.0923	0.2823	0.1027	-0.1348	0.7619	0.2135	-42.278
Cu ₂₆ -C ₁₉	0.0136	0.0289	0.0079	-0.0085	0.9260	0.2018	-2.662
C ₂₀ ...C ₁₈	0.0055	0.0168	0.0034	-0.0025	1.3358	0.1314	-0.790
H ₃₄ ...H ₃₁	0.0107	0.0404	0.0084	-0.0067	1.2485	0.1899	-2.115
N ₁₁ ...N ₁₅	0.0116	0.0464	0.0098	-0.0080	1.2249	0.1199	-2.509
H ₄₄ ...Cl ₂₇	0.0099	0.0294	0.0060	-0.0047	1.2791	0.1793	-1.481
H ₃₄ ...H ₄₁	0.0111	0.0360	0.0076	-0.0062	1.2276	0.0360	-1.940
HL1-Ni							
Ni ₂₆ -O ₂₈	0.1126	0.5991	0.1807	-0.2116	0.8538	0.1895	-66.4039
Ni ₂₆ -N ₁₁	0.1043	0.4409	0.1413	-0.1724	0.8197	0.1842	-54.0880
Ni ₂₆ -C ₁₆	0.0516	0.1186	0.0384	-0.0470	0.8153	0.2352	-14.7596
Ni ₂₆ -Cl ₂₇	0.0838	0.2605	0.0897	-0.1143	0.7848	0.2089	-35.8735
H ₃₁ ...H ₃₄	0.0105	0.0397	0.0083	-0.0066	1.2483	0.1889	-2.0804
H ₃₅ ...C ₉	0.0160	0.0524	0.0116	-0.0101	1.1501	0.1700	-3.1638
HL1-Zn							
Zn ₂₆ -O ₂₈	0.1020	0.5296	0.1573	-0.1823	0.8631	0.1813	-57.196
Zn ₂₆ -N ₁₁	0.0919	0.3845	0.1182	-0.1403	0.8426	0.1966	-44.017
Zn ₂₆ -Cl ₂₇	0.0854	0.2748	0.0912	-0.1137	0.8022	0.1999	-35.658
Zn ₂₆ -C ₁₉	0.0262	0.0503	0.0159	-0.0192	0.8269	0.2340	-6.032
Cl ₂₇ ...H ₄₄	0.0039	0.0121	0.0024	-0.0017	1.3976	0.1156	-0.531
H ₃₁ ...H ₃₄	0.0107	0.0399	0.0083	-0.0067	1.2466	0.1908	-2.096
N ₁₁ ...N ₁₅	0.0120	0.0473	0.0100	-0.0082	1.2171	0.1216	-2.585
HL1							
N ₁₇ ...H ₃₃	0.0091	0.0313	0.0063	-0.0048	1.3088	0.1794	-1.518
N ₁₁ ...N ₁₅	0.0079	0.0292	0.0058	-0.0044	1.3370	0.1550	-1.368
H ₂₉ ...H ₃₂	0.0105	0.0404	0.0084	-0.0068	1.2487	0.1892	-2.119
H ₃₂ ...H ₃₈	0.0157	0.0542	0.0117	-0.0098	1.1908	0.2036	-3.075

Table 4a: Bonding interactions and values of the electron density [$\rho(r)$] and its Laplacian [$\nabla^2 \rho(r)$], kinetic energy density [$G(r)$], potential energy density [$V(r)$] eta index, and interatomic interaction energy (E_{int}) for the bonding interactions in the HL1 complexes studied.

Citation: Julius Numbonui Ghogomu and Fritzgerald Kogge Bine. (2020). Coordination Pattern of Two Imidazole-Chalcone Hybrid Ligands and Reactivity Analysis of Their Transition Metal (II) Complexes by Density Functional Theory. *Archives of Chemistry and Chemical Engineering* 2(1).

Bonding Interaction	$\rho(r)$	$\nabla^2 \rho(r)$	$G(r)$	$v(r)$	$-G/v$	eta index	E_{int}
HL2-Co							
Co ₂₆ -O ₂₈	0.1063	0.5602	0.1660	-0.1919	0.8649	0.1789	-60.2059
Co ₂₆ -N ₁₁	0.1006	0.4275	0.1350	-0.1632	0.8275	0.1819	-51.1965
Co ₂₆ -Cl ₂₇	0.0872	0.2626	0.0925	-0.1193	0.7751	0.2108	-37.4320
Co ₂₆ -N ₁₇	0.0588	0.2122	0.0634	-0.0737	0.8600	0.1803	-23.1215
H ₃₄ ...H ₃₁	0.0107	0.0406	0.0085	-0.0068	1.2488	0.1878	-2.1267
HL2-Cu							
Cu ₂₆ -O ₂₈	0.1140	0.5430	0.1715	-0.2072	0.8276	0.1952	-65.004
Cu ₂₆ -N ₁₁	0.1068	0.3901	0.1346	-0.1717	0.7839	0.2157	-53.876
Cu ₂₆ -Cl ₂₇	0.0929	0.2838	0.1035	-0.1361	0.7607	0.2139	-42.704
Cu ₂₆ -C ₁₉	0.0131	0.0278	0.0075	-0.0081	0.9288	0.2020	-2.546
C ₂₀ ...C ₁₉	0.0059	0.0175	0.0035	-0.0027	1.3128	0.1291	-0.843
N ₁₁ ...N ₁₅	0.0116	0.0462	0.0098	-0.0080	1.2265	0.1193	-2.496
Cl ₂₇ ...H ₄₄	0.0100	0.0297	0.0061	-0.0048	1.2803	0.1798	-1.491
H34...H ₄₁	0.0111	0.0361	0.0076	-0.0062	1.2282	0.2062	-1.943
H ₃₄ ...H ₃₁	0.0109	0.0411	0.0086	-0.0069	1.2476	0.1907	-2.156
HL2-Ni							
Ni ₂₆ -O ₂₈	0.1120	0.5953	0.1794	-0.2100	0.8543	0.1886	-65.8946
Ni ₂₆ -N ₁₁	0.1046	0.4433	0.1420	-0.1732	0.8200	0.1839	-54.3389
Ni ₂₆ -C ₁₆	0.0538	0.1229	0.0403	-0.0498	0.8086	0.2374	-15.6184
Ni ₂₆ -Cl ₂₇	0.0841	0.2609	0.0900	-0.1148	0.7840	0.2086	-36.0277
Cl ₂₇ ...H ₃₉	0.0113	0.0364	0.0076	-0.0061	1.2438	0.1784	-1.9175
C ₉ ...H ₃₅	0.1784	0.0404	0.0084	-0.0068	1.2471	0.1898	-2.1200
H ₃₁ ...H34	0.0158	0.0530	0.0117	-0.0101	1.1539	0.1705	-3.1758
HL2-Zn							
Zn ₂₆ -O ₂₈	0.1030	0.5382	0.1600	-0.1854	0.8629	0.1814	-58.162
Zn ₂₆ -N ₁₁	0.0895	0.3756	0.1146	-0.1352	0.8473	0.1950	-42.416
Zn ₂₆ -Cl ₂₇	0.0899	0.2883	0.0972	-0.1224	0.7945	0.2023	-38.396
Zn ₂₆ -C ₁₆	0.0193	0.0364	0.0112	-0.0133	0.8411	0.2194	-4.188
Cl ₂₇ ...C ₁₉	0.0082	0.0248	0.0051	-0.0041	1.2588	0.1376	-1.282
C ₉ ...H ₃₅	0.0164	0.0583	0.0129	-0.0111	1.1539	0.1599	-3.495
H ₃₁ ...H ₃₄	0.0109	0.0405	0.0085	-0.0068	1.2461	0.1914	-2.130
HL2							
H ₃₈ ...H ₃₂	0.0162	0.0545	0.0118	-0.0099	1.1863	0.2134	-3.112
H ₃₂ ...H ₂₉	0.0108	0.0411	0.0086	-0.0069	1.2469	0.1905	-2.158
N ₁₇ ...H ₃₃	0.0097	0.0338	0.0069	-0.0053	1.3008	0.1762	-1.653
N ₁₅ ...N ₁₁	0.0080	0.0306	0.0061	-0.0046	1.3386	0.1487	-1.430

Table 4b: Bonding interactions and values of the electron density [$\rho(r)$] and its Laplacian [$\nabla^2 \rho(r)$], kinetic energy density [$G(r)$], potential energy density [$V(r)$] eta index, and interatomic interaction energy-y (E_{int}) for the bonding interactions in the HL2 complexes studied.

Citation: Julius Numbonui Ghogomu and Fitzgerald Kogge Bine. (2020). Coordination Pattern of Two Imidazole-Chalcone Hybrid Ligands and Reactivity Analysis of Their Transition Metal (II) Complexes by Density Functional Theory. *Archives of Chemistry and Chemical Engineering* 2(1).

As can be seen from Table 4 and the molecular graphs, the M-L interactions: $\text{Co}_{26}\cdots\text{C}_{16}$, $\text{Co}_{26}\cdots\text{N}_{17}$, $\text{Cu}_{26}\cdots\text{C}_{19}$, $\text{Ni}_{26}\cdots\text{C}_{16}$, $\text{Zn}_{26}\cdots\text{C}_{19}$, $\text{Zn}_{26}\cdots\text{C}_{16}$ are identified in the complexes studied via QTAIM analysis, thus corroborating the fact that the imidazole ring can bind to central metal atoms/ions through variable donor sites. QTAIM analysis, in total agreement with the conceptual DFT-based reactivity indices and molecular electrostatic (MEP) potential maps, has also shown that the carbon atoms of the imidazole ring, as opposed to the nitrogen atom N17, are the most favorable electron donors (or coordination sites) to central metal ions. Interestingly, QTAIM analysis has revealed some M-L interactions, $\text{Cu}_{26}\cdots\text{C}_{19}$ (in HL1 and HL2 complexes) and $\text{Zn}_{26}\cdots\text{C}_{16}$ (in HL2 complexes), that were apparently missed by geometry optimization. The energies of the latter interactions (which fall in the range -2.546 to -4.188 kcal/mol) are by far smaller than those of the other interactions listed above (ranging from -6.032 to -23.122 kcal/mol), and can be considered as weak van der Waals interactions instead of M-L coordinate bonds. Other M-L interactions not involving the imidazole ring have been identified by QTAIM analysis, as can be seen from Table 4. Topological analysis of the electron density has also shown an interplay of non-covalent intramolecular interactions in the molecules investigated, including: HBs, halogen bonds, van der Waals and H \cdots H interactions. Although the interaction energies of these interactions are small as evidenced in Table 4, their collective effect on the stability and shapes of the molecules cannot be underestimated. Among these, the halogen bond $\text{Cl}_{27}\cdots\text{C}_{19}$ in HL2-Zn, is very interesting because it involves the most nucleophilic carbon atom in the imidazole ring of HL2, as earlier predicted by the local nucleophilicity index (N_{L}) tool.

Non-covalent interaction (NCI) analysis of studied compounds

To ensure a comprehensive elucidation of the non-covalent interactions in the compounds investigated herein, Bader's QTAIM analysis has been complemented with the recently developed method for probing non-covalent interactions in real space known as the non-covalent interaction (NCI) index. The latter is also known as the reduced density gradient (RDG) method, which has become very popular and is routinely used for studying weak interactions. It is based on the peaks that appear in the RDG at low densities. Indeed, NCIs play crucial roles in the study of many chemical and biological systems ranging from protein-ligand interaction to structural integrity and stability of molecular systems [46]. The NCI index detects non-covalent interactions in real space on the basis of the electron

density and its derivatives with very little dependence on the method and basis set used in the calculation of the electron density [47], as shown in Equation (8).

$$s = \frac{1}{2(3\pi^2)^{1/3}} \frac{|\nabla\rho|}{\rho^{4/3}} \quad (8)$$

The NCI index also has the advantage that it permits the visualization of weak interactions in real space by means of 3D isosurfaces and 2D scatter plots of RDG (s) against $\text{sign}[\lambda_2(r)]\rho(r)$. Herein, the characterization of non-covalent interactions is facilitated via the analysis of the sign of the second eigen value (λ_2) of the electron density hessian matrix. To facilitate the interpretation of results, a color code (Figure 4) corresponding to different types and strengths of non-covalent interactions is usually mapped onto the 3D RDG isosurfaces, and sometimes onto the 2D scatter plots.

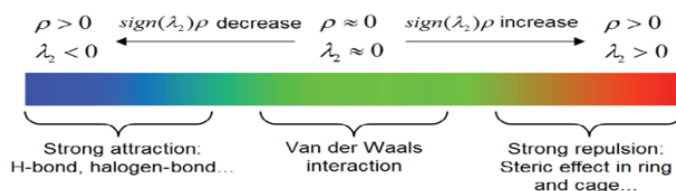


Figure 4: Color code showing types of weak interaction present and their relative strength.

The grid data of RDG and $\text{sign}(\lambda^2)\rho$ calculated with Multiwfn, and subsequently used for NCI analysis in VMD v.1.9.2 [48], was based on self-consistent-field (SCF) generated densities at the geometry of the gas phase optimized molecules studied herein. A careful inspection of the RDG scatter plots corresponding to all investigated complexes (see Figures 5a and 5b plotted using the gnuplot 5.2 software) reveals the existence of spikes at the base of each plot, which confirm the presence of weak non-covalent interactions in each of the complexes. Based on the color code associated with the scatter plots, it has been observed that the complexes HL1-Zn, HL2-Ni, HL2-Co and HL2-Zn possess weak to fairly strong attractive non-covalent interactions with $\text{sign}(\lambda^2)\rho(r)$ values -0.026, -0.020, -0.020 and -0.020 respectively. This is a clear indication that some attractive non-covalent interactions in HL1-Zn are relatively stronger than those in the other complexes. On the other hand, strongly repulsive van der Waals interactions are also found to exist in all of the complexes under study.

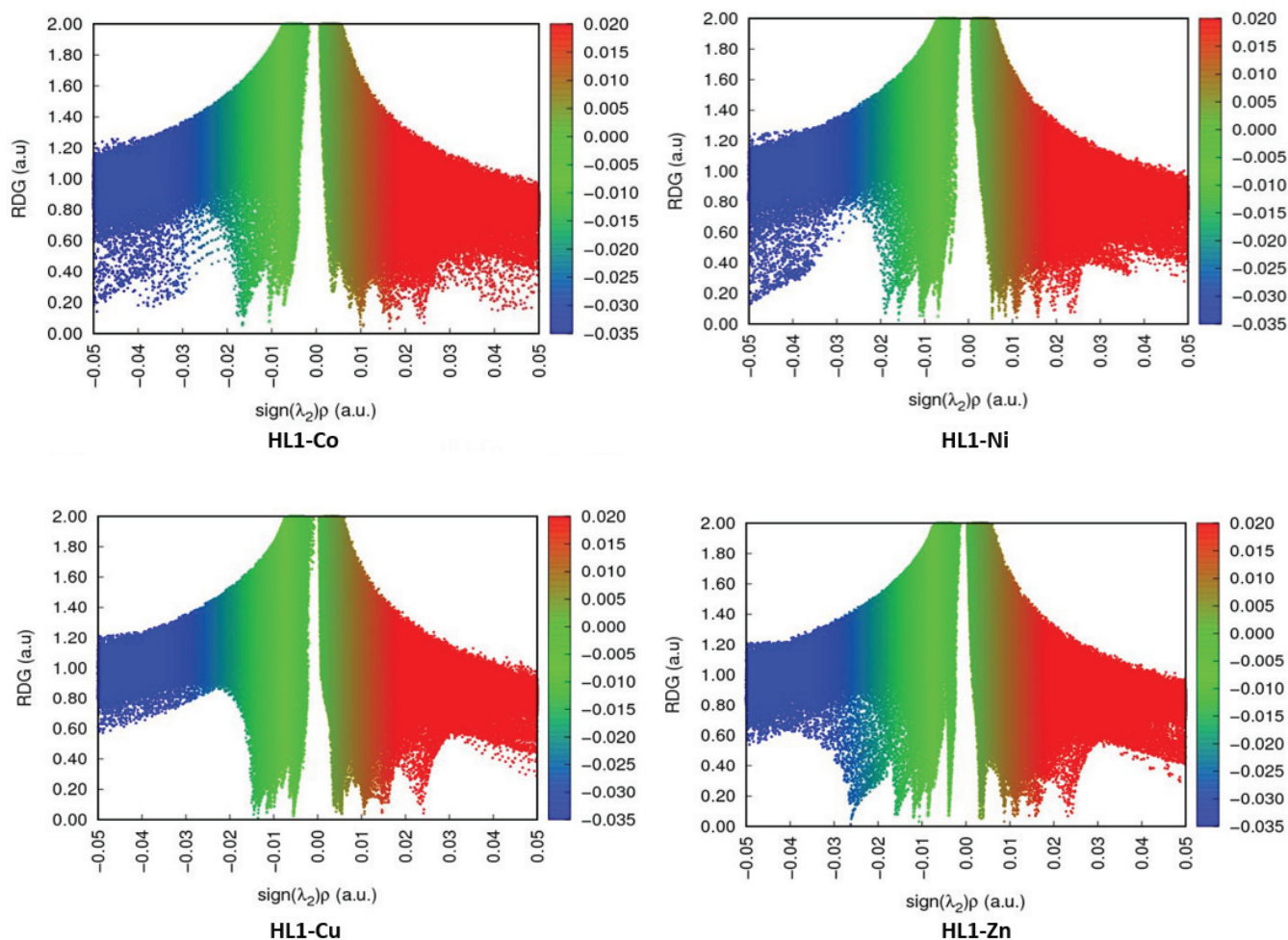


Figure 5a: RDG maps of HL1 complexes in gas phase based on optimized structures at the RI-BP86-D3(BJ)/def2-TZVP level of theory

To easily locate and describe the nature and strengths the aforementioned information from the RDG plots, the 3D RDG isosurfaces of the complexes are visualized as shown in Figures 6a and 6b using VMD at 0.500 a.u. isosurface value. It is noteworthy that the color codes used for the scatter plots and the isosurfaces are identical. As can be observed, the van der Waals forces play an important role in the structural stability of the complexes especially around the imidazole ring and other parts of the complexes. The isosurfaces clearly show that the aforementioned attractive non-covalent interactions are localized in the vicinity of the organometallic bonds

observed in the concerned complexes. The QTAIM-revealed H...H and H...Cl interactions in the complexes are essentially weak van der Waals forces, as shown in Figures 6a and 6b.

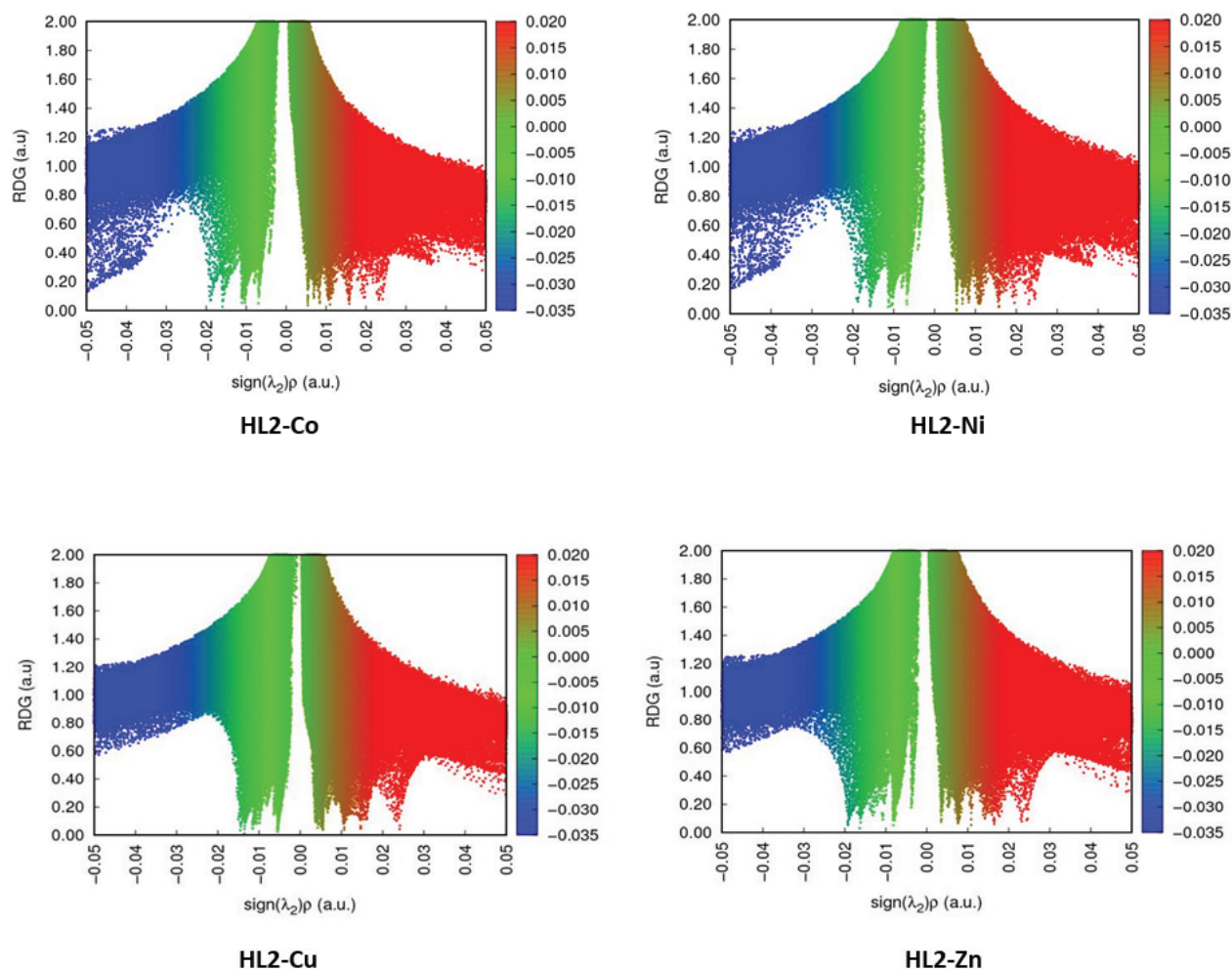


Figure 5b: RDG maps of HL2 complexes in gas phase based on optimized structures at the RI-BP86-D3 (BJ)/def2-TZVP level of theory.

Interestingly, RDG isosurfaces are found to exist between the central metal ion and the imidazole moiety in all investigated complexes, which can be attributed to covalent and non-covalent interactions between each metal ion and variable binding in the moiety. It is equally important to note that the NCI index tool has transcended QTAIM analysis by elucidating $\text{Cl}_{27} \cdots \text{C}_{19}$ halogen bonds in all complexes studied, whereas the latter approach has shown the existence of this interaction in HL2-Zn only. This further confirms the strongly nucleophilic nature of the carbon atom C_{19} in all the investigated complexes, as earlier predicted by the N_k index.

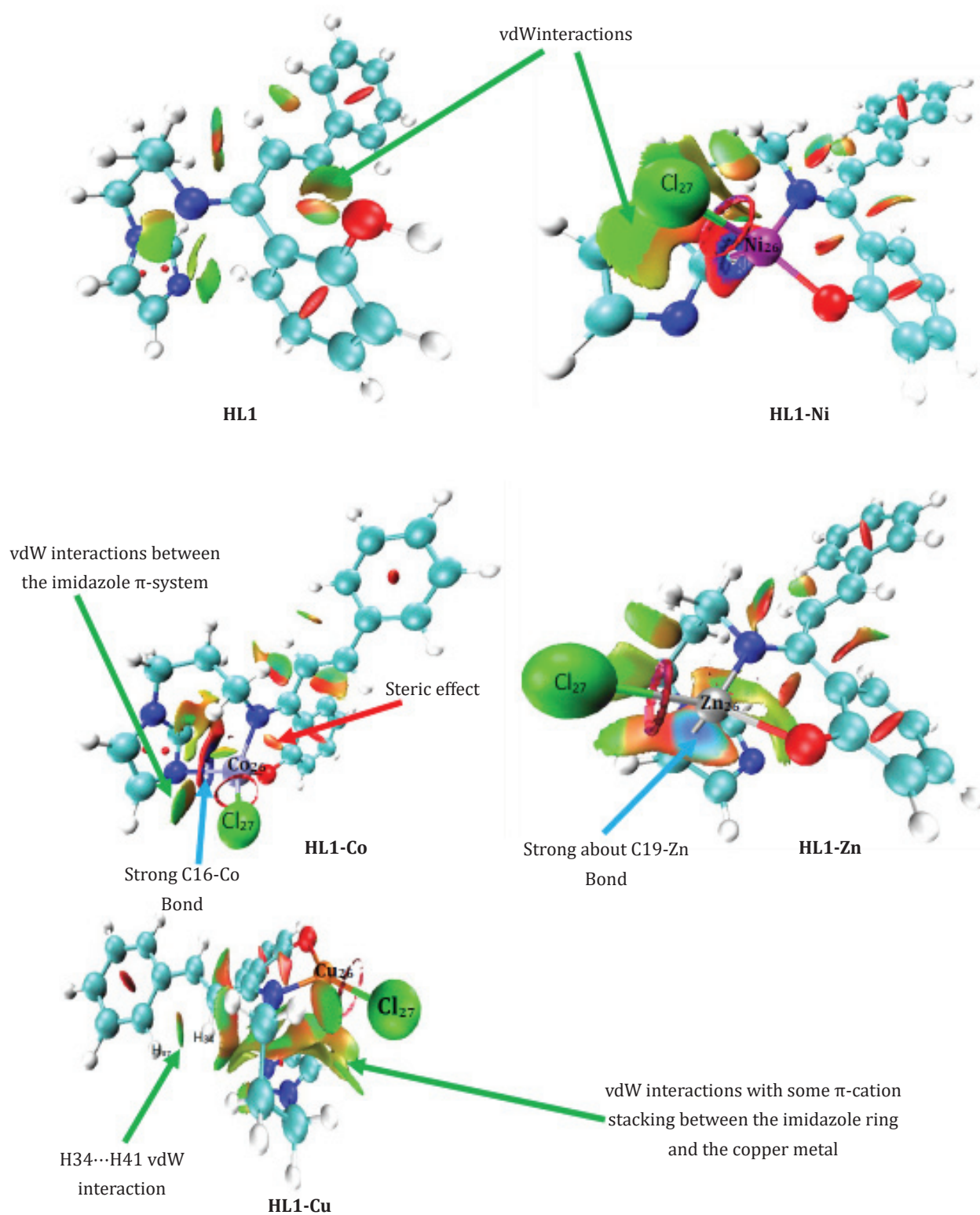


Figure 6a: Annotated 3D NCI isosurfaces of HL1 complexes obtained with the VMD v.1.9.2 visualization software at isosurface value 0.5

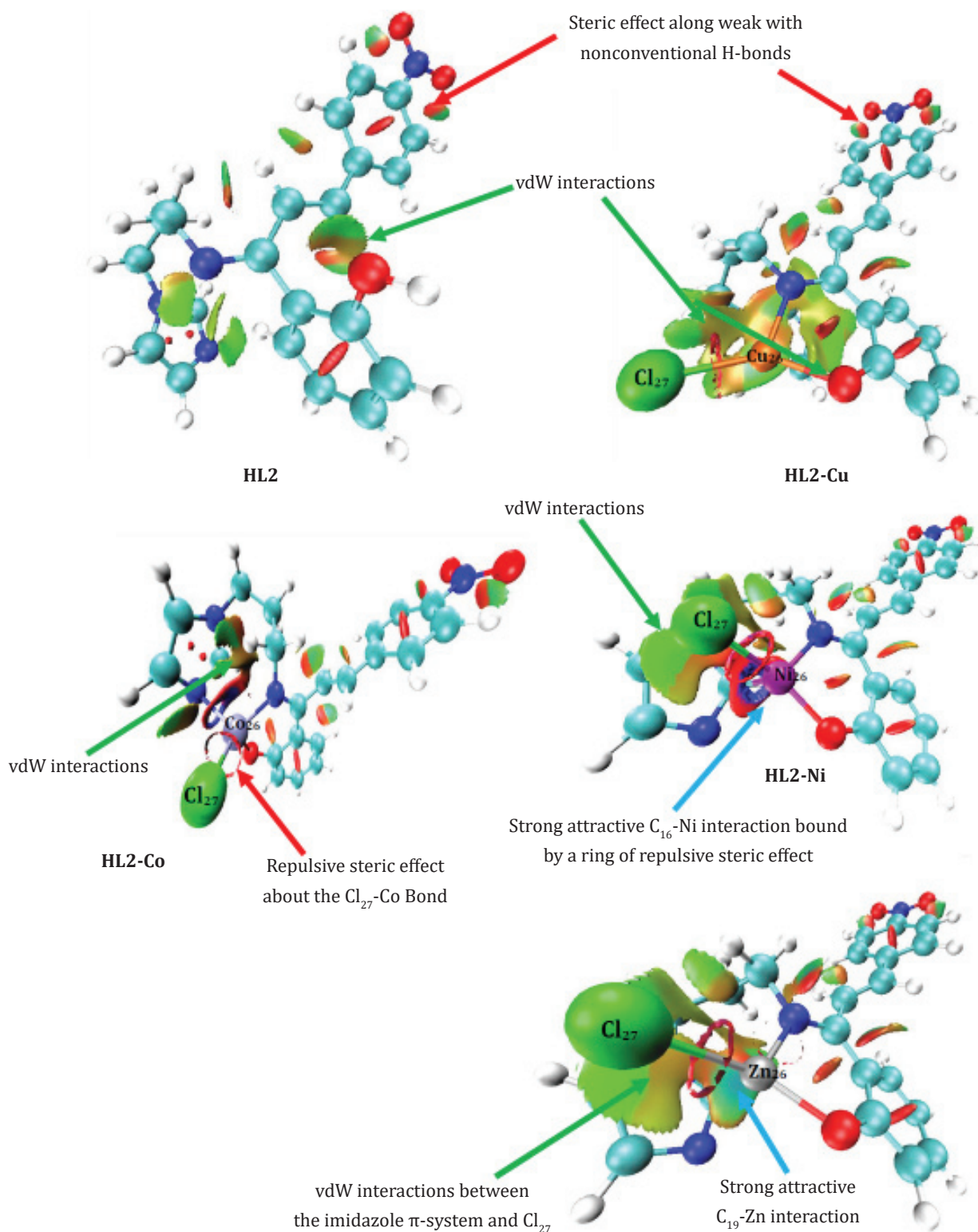


Figure 6b: Annotated 3D NCI isosurfaces of HL2 complexes obtained with the VMD v.1.9.2 visualization software at isosurface value 0.5

Citation: Julius Numbonui Ghogomu and Fitzgerald Kogge Bine. (2020). Coordination Pattern of Two Imidazole-Chalcone Hybrid Ligands and Reactivity Analysis of Their Transition Metal (II) Complexes by Density Functional Theory. *Archives of Chemistry and Chemical Engineering* 2(1).

Chemical reactivity analysis

Global reactivity tendencies of the compounds studied

In the realm of conceptual DFT (CDFT) relevant concepts and principles used in predicting the chemical behavior of molecules are conveniently extracted from the electron density, in terms of global reactivity descriptors (GRDs) and local reactivity descriptors (LRDs). While the LRDs used in this study had been highlighted earlier, the GRDs used include: chemical potential (μ), global hardness (η), global softness (S), electrophilicity index (ω) and electronegativity (χ). These GRDs are calculated as follows:

$$\chi = -\mu = 1/2 (IP_v + EA_v) \quad (9)$$

$$\eta = 1/2 (IP_v - EA_v) \quad (10)$$

$$\omega = \mu^2/2\eta \quad (11)$$

In these Equations (9 and 10), the ionization potential (IP) and electronic affinity (EA) are obtained as follows:

$$IP_v = E_{N-1} - E_N \quad (12)$$

$$EA_v = E_N - E_{N+1} \quad (13)$$

Where E_N , E_{N-1} and E_{N+1} are the single point energies of the neutral, cationic, and anionic forms of the N-electron system for the optimized geometry of the neutral molecule. The electronic chemical potential, μ , is associated with the feasibility of a system to exchange electron density with the environment at the ground state. The electronegativity, χ , is a measure of the resistance to electron density loss. The chemical hardness, η , is thought of as the resistance of a molecule to electron density exchange with the environment. The global electrophilicity index, ω , which is a measure of the energy stabilization of a molecule when it acquires an additional amount of electron density, is one of the most important reactivity indices [39].

The values of the GRDs computed (in gas phase) in this work are reported in Table 5. It is clear from Table 5 that ligand HL2 is a stronger electrophile than its HL1 counterpart and, as a consequence, more chemically reactive than the latter. This trend is explained by the fact that HL1 is chemically harder and thus less reactive than HL2. Similarly, the transition metal complexes of HL2 are more electrophilic than the corresponding complexes of HL1, which imply that the former are more reactive. It must be pointed out that the Cu(II) complexes of both ligands remarkably more reactive than the other

complexes, which is apparently responsible for their marked antifungal activities as reported in [12] based on experimental studies. Although metal ion coordination reduces chemical hardness (or increases chemical softness) in all cases investigated, a corresponding improvement in electrophilicity and thus chemical reactivity is noticeable only in the case of the Cu (II) complexes.

Compound	μ	χ	η	ω
HL1-Co	-4.106	4.106	3.026	25.504
HL1-Cu	-5.293	5.293	2.862	40.084
HL1-Ni	-4.521	4.521	2.687	27.455
HL1-Zn	-4.291	4.291	3.027	27.863
HL1	-4.310	4.310	3.699	34.349
HL2-Co	-4.652	4.652	2.723	29.468
HL2-Cu	-5.562	5.562	2.844	44.000
HL2-Ni	-4.954	4.954	2.780	34.112
HL2-Zn	-4.846	4.846	2.752	32.305
HL2	-4.971	4.971	3.318	40.989

Table 5: Global Reactivity Descriptors (GRD) of the complexes investigated in eV calculated at RIJCOSX-M06/ma-def2-TZVP level of theory for the complexes and RIJCOSX-M062X/ma-def2-TZVP level of theory for the ligands, all in gas phase.

Local reactivity patterns within the complexes studied

In order to identify reactive sites in the complexes currently studied that are susceptible to attack by electrophilic and nucleophilic species, the LRDs and molecular electrostatic potential (MEP) maps have been computed at RIJCOSX-M06/def2-TZVP level of theory based on the optimized structures of the complexes. The computed LRDs and MEPs are presented in Table 6 and Figure 7, respectively. It is clear from Table 6 that apart from the Zn (II) complexes, the metal ion center in all investigated complexes are liable to attack by nucleophiles. Consequently, more ligand species (usually nucleophiles) can bind to these metallic centers via their unoccupied coordination sites resulting in complexes with coordination numbers greater than four. It turns out that the Cu (II) ion centers are the most susceptible to nucleophilic attack, which greatly contributes to the high reactivity of its complexes with HL1 and HL2. From the f_k^- values in Table 6, it is unequivocally clear that the carbon and oxygen atoms of the phenolic moiety, along with the chloride ligands in all investigated complexes are the most favorable sites for attack by electrophiles. Expectedly, the f_k^- values have shown that the oxygen atoms of the nitro group ($-\text{NO}_2$) are less receptive

to electrophiles than the phenolic oxygen atoms. This can be attributed to the extensive electron delocalization within the -NO₂ group and beyond, which renders the lone electron pairs in the valence shells of these oxygen atoms less available to electrophiles. In the

case of the phenolic oxygen, the effect of electron delocalization on the availability of its lone pairs of electrons is minimal. Apparently, the Zn (II) ion in its complexes may act as an ambiphilic center that is prone to attack by both electrophiles and nucleophiles.

Atom	HL1-Co		HL1-Ni		HL1-Cu		HL1-Zn	
	f_k^-	f_k^+	f_k^-	f_k^+	f_k^-	f_k^+	f_k^-	f_k^+
2 C	0.023	0.034	0.022	0.022	0.030	0.025	0.025	0.061
3 C	0.012	0.016	0.012	0.010	0.014	0.012	0.013	0.027
4 C	0.012	0.018	0.012	0.012	0.015	0.013	0.012	0.032
5 C	0.008	0.016	0.008	0.009	0.013	0.011	0.008	0.033
6 C	0.005	0.014	0.005	0.005	0.010	0.007	0.008	0.034
7C	-0.007	0.001	-0.007	-0.006	-0.001	-0.006	-0.006	0.015
8C	0.015	0.036	0.015	0.023	0.022	0.029	0.015	0.073
9C	-0.016	0.003	-0.015	-0.014	-0.002	-0.013	-0.011	0.044
10 C	0.009	0.047	0.009	0.030	0.007	0.027	0.004	0.060
11 N	0.031	0.014	0.025	-0.009	0.033	0.006	0.024	0.049
12 C	0.008	0.006	0.008	0.004	0.010	0.008	0.008	0.010
13 C	0.007	0.005	0.006	0.003	0.007	0.004	0.006	0.007
14 C	0.006	0.007	0.005	0.006	0.005	0.003	0.005	0.005
15 N	0.008	0.015	0.008	0.022	0.008	-0.001	0.006	0.001
16 C	0.000	0.015	0.005	-0.007	0.025	0.014	0.011	-0.001
17 N	0.005	0.015	0.012	0.048	0.014	0.016	-0.001	0.006
18 C	0.010	0.016	0.027	0.036	0.022	0.011	0.003	0.008
19 C	0.018	0.026	0.035	0.053	0.026	-0.010	0.017	0.008
20 C	0.061	0.006	0.056	0.006	0.037	0.007	0.064	-0.003
21 C	0.038	0.020	0.038	0.018	0.023	0.018	0.040	0.010
22 C	0.102	0.035	0.098	0.033	0.078	0.034	0.110	0.020
23 C	0.034	0.039	0.032	0.033	0.030	0.033	0.035	0.040
24 C	0.069	0.024	0.068	0.017	0.054	0.019	0.075	0.022
25C	0.045	0.015	0.042	0.008	0.031	0.007	0.052	0.023
26 M	0.035	0.143	0.028	0.260	0.007	0.310	0.022	0.024
27 Cl	0.087	0.093	0.071	0.092	0.121	0.147	0.049	0.037
28 O	0.104	0.032	0.097	0.010	0.078	0.042	0.117	0.028

Table 6a: Values of the condensed Fukui functions (f_k^- , f_k^+ , f_k^0) HL1 complexes (all values in a.u.).

Atom	HL2-Co		HL2-Ni		HL2-Cu		HL2-Zn	
	f_k^-	f_k^+	f_k^-	f_k^+	f_k^-	f_k^+	f_k^-	f_k^+
1N	0.004	0.052	0.004	0.034	0.005	0.011	0.004	0.052
2 C	0.016	0.032	0.016	0.021	0.020	0.018	0.016	0.036
3 C	0.008	0.030	0.008	0.019	0.010	0.011	0.008	0.031
4 C	0.009	0.039	0.009	0.024	0.010	0.012	0.008	0.040
5 C	0.008	0.029	0.007	0.018	0.011	0.012	0.007	0.032
6 C	0.003	0.030	0.004	0.016	0.007	0.008	0.005	0.033
7C	-0.010	0.039	-0.010	0.018	-0.008	-0.003	-0.010	0.041
8C	0.019	0.031	0.017	0.021	0.023	0.028	0.015	0.039
9C	-0.025	0.053	-0.018	0.017	-0.010	-0.010	-0.018	0.057
10 C	0.015	0.013	0.014	0.017	0.009	0.025	0.008	0.025
11 N	0.033	0.015	0.037	-0.003	0.034	0.005	0.028	0.028
12 C	0.009	0.003	0.009	0.004	0.010	0.008	0.008	0.005
13 C	0.007	0.002	0.006	0.002	0.007	0.004	0.006	0.003
14 C	0.006	0.005	0.005	0.005	0.005	0.003	0.005	0.003
15 N	0.009	0.005	0.006	0.014	0.009	-0.001	0.008	-0.001
16 C	-0.001	0.003	0.011	-0.007	0.028	0.012	0.017	-0.007
17 N	0.005	0.009	0.009	0.031	0.015	0.015	0.013	0.008
18 C	0.012	0.010	0.027	0.027	0.024	0.010	0.036	0.011
19 C	0.018	0.012	0.031	0.036	0.027	-0.009	0.043	0.010
20 C	0.060	0.000	0.049	0.005	0.038	0.006	0.053	-0.001
21 C	0.041	0.003	0.035	0.009	0.024	0.016	0.037	0.001
22 C	0.101	0.019	0.086	0.025	0.079	0.031	0.094	0.014
23 C	0.034	0.023	0.032	0.025	0.030	0.032	0.031	0.026
24 C	0.070	0.019	0.059	0.016	0.054	0.018	0.063	0.017
25C	0.043	0.009	0.035	0.007	0.031	0.007	0.042	0.016
26 M	0.028	0.047	0.008	0.160	0.007	0.291	0.021	0.016
27 Cl	0.087	0.036	0.110	0.065	0.124	0.138	0.054	0.027
28 O	0.107	0.022	0.100	0.016	0.079	0.041	0.096	0.021
48 O	0.019	0.093	0.017	0.060	0.019	0.028	0.017	0.094
49 O	0.017	0.093	0.018	0.061	0.021	0.029	0.018	0.094

Table 6b: Values of the condensed Fukui functions (f_k^- , f_k^+ , f_k^0) HL2 complexes (all values in a.u.)

In order to supplement the findings obtained from the LRDs and also to visualize the different reactive sites within the investigated complexes, their MEP maps (see Figure 7) were computed at RIJ-COSX-M06/def2-TZVP level of theory in gas phase. In these maps, the color code: red to yellow indicates regions of low electrostatic potential and are related to electrophilic reactivity, while blue to

green indicates regions of high electrostatic potential related to nucleophilic reactivity sites. It must be pointed out that this color code gives us an insightful idea of the eventual electrostatic complementarities between investigated potential drug candidates and some target biological molecules, hence giving a predictive value in drug design [49].

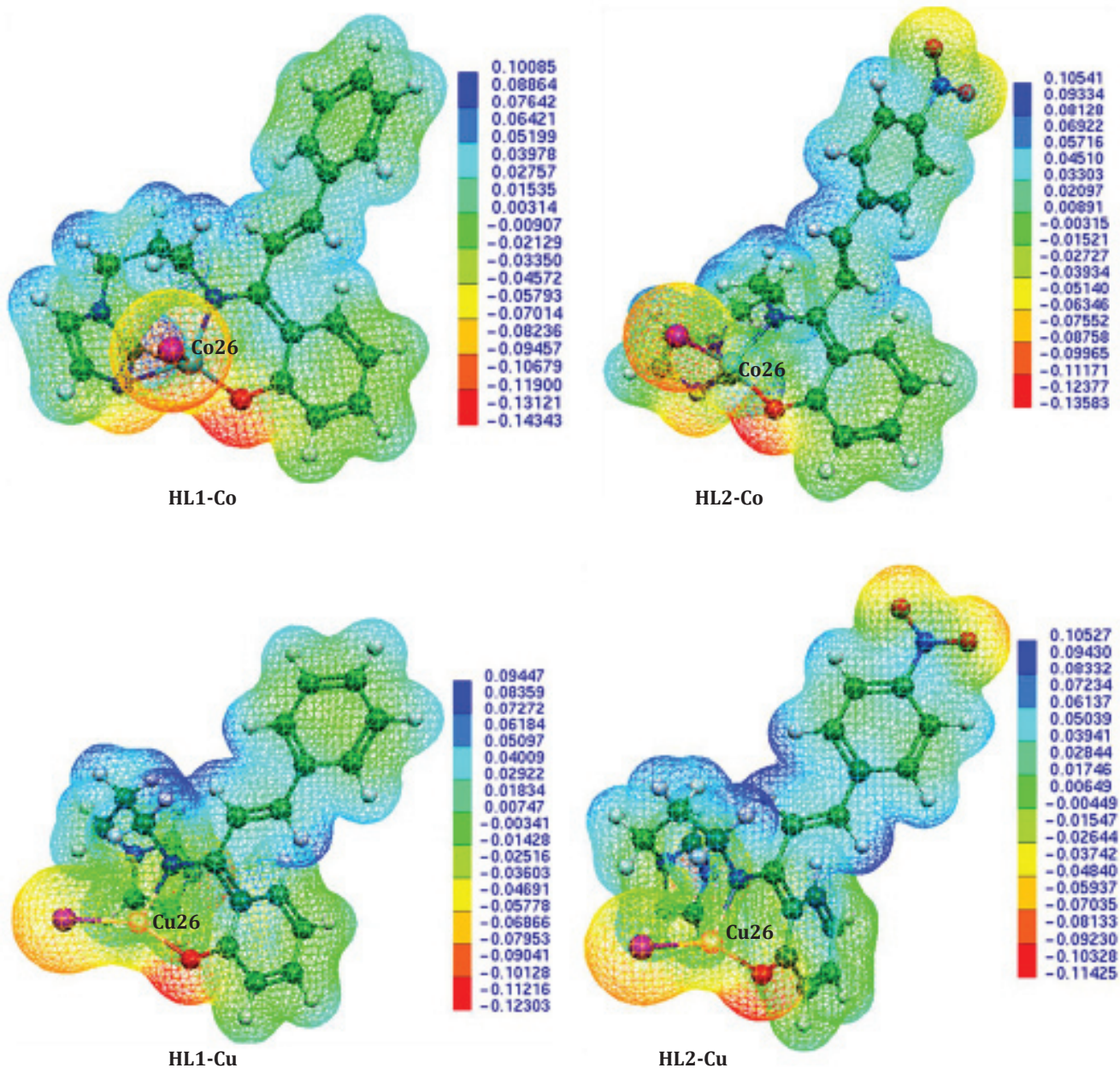


Figure 7a: Molecular electrostatic potential (MEP) surfaces of Co (II) and Cu (II) complexes, mapped onto electron density isosurfaces of value 0.01 a.u., using Molekel 4.3.

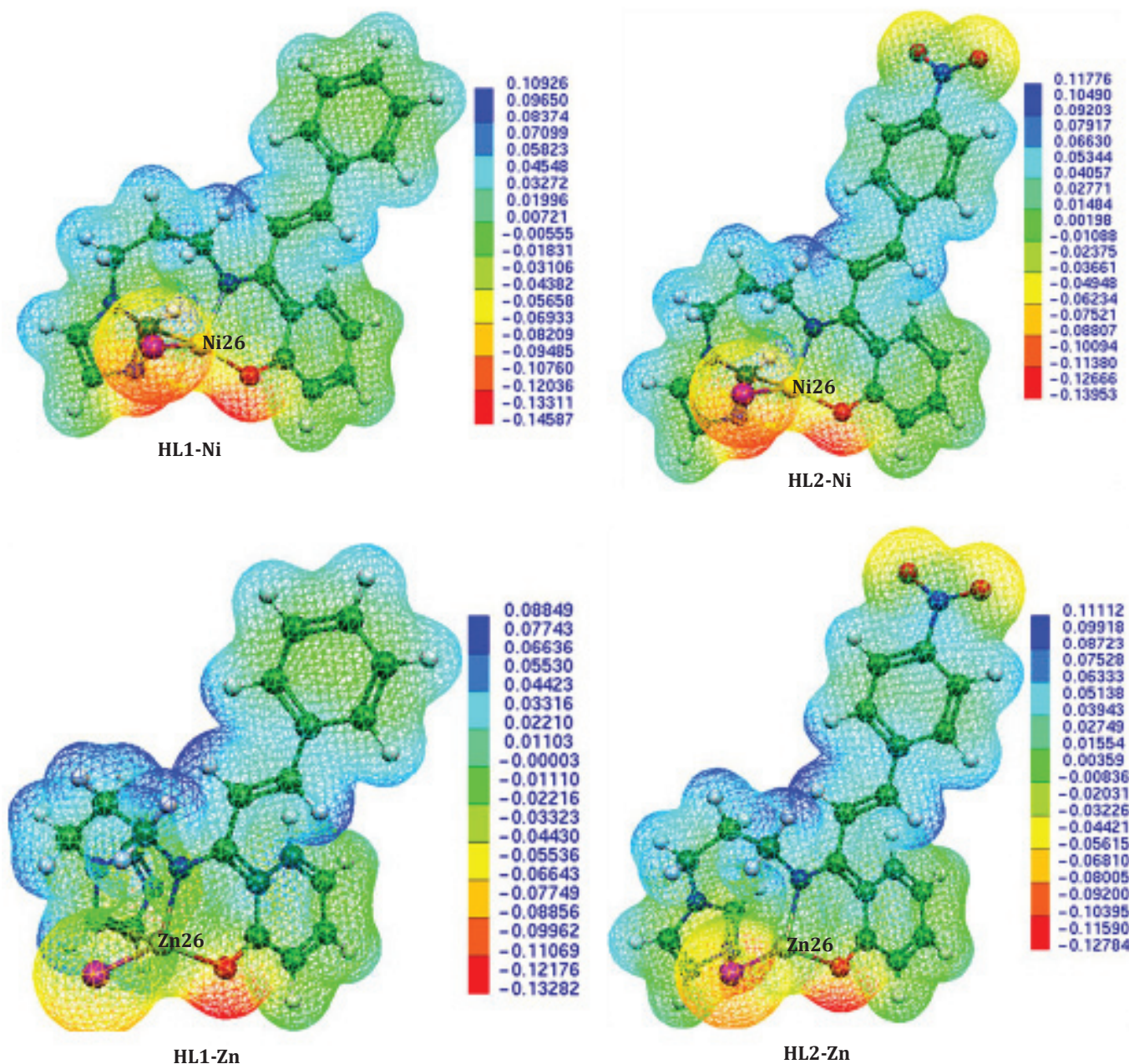


Figure 7b: Molecular electrostatic potential (MEP) surfaces of Ni(II) and Zn(II) complexes, mapped onto electron density isosurfaces of value 0.01 a.u., using Molekel 4.3.

It is clear from the MEP maps of all complexes that the phenolic oxygen, the chloride ligand, the N17 nitrogen of the imidazole ring and, to a lesser extent, the carbon atoms of the phenolic moiety are the most favorable sites for electrophilic attacks, since they are associated with the reddish, orange and yellowish MEP regions. Apparently, the hydrogen atoms of the N-(3-aminopropyl) and ethylenic groups are highly acidic as they are associated blue-colored MEP regions, and as such are susceptible to attack by nucleophiles. Consequently, these hydrogen atoms can easily get involved in both intra- and inter-molecular hydrogen bond formations within the complexes. Such intermolecular hydrogen atoms could be formed with nucleophilic sites in protein molecules present in microorganisms, resulting in interference with the normal cell processes. It is clear from the maps that the oxygen atoms of the nitro group are indeed less receptive to electrophiles than the phenolic oxygen atoms, as earlier shown by the LRDs.

Conclusion

In order to carry out quantitative structure activity relationships (QSAR) studies in view of enhancing the bioactivities of chalcone-imidazole hybrids, detailed knowledge of the structural and reactivity potentials of these molecules is required. Unfortunately, comprehensive structural and reactivity studies on these molecules are uncommon, reason for which the present work has been carried out. In this work, structural and chemical reactivity studies on two chalcone-containing Schiff bases of N-(3-aminopropyl) imidazole and their transition metal complexes have been performed using the DFT method. The results obtained clearly reveal that both HL1 and HL2 can act as tridentate chelating ligands toward the metal (II) ions investigated, except the Cu (II) ion, in which case they act as bidentate ligands. Furthermore, both ligands are found to utilize variable electron donor sites localized within the imidazole ring to coordinate with metal ions. These observations are somewhat contrary to some earlier reports, which showed that HL1 and HL2 can only act as tridentate ligands bearing a unique set of donor atoms toward metal (II) ions. Interestingly, the Ni (II) complexes of both ligands and the Zn (II) complex of HL1 are found to be organometallic in nature. A network of non-covalent intramolecular interactions was identified in the complexes studied. HL2 and its complexes are found to be more reactive than their HL1 counterparts, owing to their higher electrophilicity indices. Results have also shown that apart from the Zn (II) complexes, the metal ion center in all investigated complexes are liable to attack by nucleophiles. The Cu (II) ion center is found to be most susceptible to nucleophilic attack, and

this certainly contributes to the higher reactivity of its complexes with HL1 and HL2. Furthermore, it is clear from the results that the carbon and oxygen atoms of the phenolic moiety, along with the chloride ligands in all investigated complexes are the most favorable sites for attack by electrophiles. Finally, the structural diversity, coordination behavior and reactivity patterns of some imidazole-based chalcones as rationalized in this work, can open new avenues in the fight against drug resistance.

Acknowledgements

The authors gratefully acknowledge the material support from the Research Unit of Noxious Chemistry and Environmental Engineering of the University of Dschang, Cameroon.

References

1. Chavan B.B., Gadekar A. S., Mehta P.P., Vawhal P.K., Kolsure A.K. and Chabukswar, A.R. (2016). Synthesis and Medicinal Significance of Chalcones-A Review. *Asian J. biomed. Pharm. Sci.* 6(56): 01-07.
2. Suwito H., Jumina M., Alfinda N.K. and Ni N.T.P. (2014). Chalcones: Synthesis, structure diversity and pharmacological aspects. *J. Chem. Pharm. res.*, 6(5): 1076-1088.
3. Singh P., Anand A., Kumar V. (2014). Recent developments in biological activities of chalcones: A mini review. *Eur. J. Med. Chem.*, 85:758-777.
4. Andrew S. Jr. and Cock C. H. (1981). *Introduction to Organic Chemistry*. 2nd Edition, Macmillan Publishing Co., Inc., New York.
5. Sirsat S.B., Halikar N.K., Pund M.M. and Vartale S.P. (2012). Synthesis and Biological Screening of Some Novel Hetero-Aryl Chalcone and their complexes. *J. pharm. Bio. Chem. Sci.*, 3(2): 240.
6. Shibata S. (1994). Anti-tumorigenic Chalcones. *J. Stem Cells*, 12: 44-52.
7. Soloman V.R., Hu C. and Lee H. (2009). Hybrid pharmacophore design and synthesis of isatin-benzothiazole analogs for their anti-breast cancer activity. *Bioorg. Med. Chem.*, 17: 7585-7592.
8. Luca De L. (2006). Naturally Occurring and Synthetic Imidazoles: Their Chemistry and Their Biological Activities. *Curr. Med. Chem.*, 13:1-23.
9. Zhang L., Peng X., Damu G. L.V., Geng R. and Zhou C. (2014). Comprehensive Review in Current Developments of Imidazole-Based Medicinal Chemistry. *Med. Res. Rev.*, 34(2): 340-437.

Citation: Julius Numbonui Ghogomu and Fitzgerald Kogge Bine. (2020). Coordination Pattern of Two Imidazole-Chalcone Hybrid Ligands and Reactivity Analysis of Their Transition Metal (II) Complexes by Density Functional Theory. *Archives of Chemistry and Chemical Engineering* 2(1).

10. Zhou C.H., Gan L.L., Zhang Y.Y., Zhang F.F., Wang G.Z., Jin L. and Geng R.X. (2009). Review on supermolecules as chemical drugs. *Sci. China Ser. B.*, 52: 415–458.
11. Zhou C.H., Zhang Y.Y., Yan C.Y., Wan K., Gan L.L. and Shi Y. (2010). Recent researches in metal supramolecular complexes as anti-cancer agents. *Anti-cancer Agents Med. Chem.*, 10: 371–395.
12. Kalanithi M., Rajarajan M., Tharmaraj P. and Sheela C.D. (2012). Spectral, biological screening of metal chelates of chalcone based Schiff bases of N-(3-aminopropyl) imidazole. *Spectrochim. Acta A*, 87, 155–162.
13. Mary C.P.V., Shankar R. and Vijayakumar S. (2019). Theoretical insights into the metal chelating and antimicrobial properties of the chalcone based Schiff bases. *Mol. Simulat.*, 45(8): 636–645.
14. Guo N., Maurice R., Teze D., Graton J., Champion J., Montavon G. and Galland N. (2018). Experimental and computational evidence of halogen bonds involving astatine. *Nat. Chem.*, 10: 428–434.
15. Nogrady T. and Weaver D. F. (2005). *Medical Chemistry: A molecular and Biochemical Approach*. 3rd Edition, Oxford University Press, Oxford.
16. Orto M., Pantazis D.A. and Neese F. (2009). Density functional theory. *Photosynth. Res.*, 102: 443–453.
17. Neese F. (2009). Prediction of molecular properties and molecular spectroscopy with density functional theory: From fundamental theory to exchange-coupling. *Coord. Chem. Rev.*, 253, 526–563.
18. Neese F. (2012). The ORCA program system. *Wiley Interdiscipl. Rev. Comput. Mol. Sci.*, 2: 73–78.
19. Hanwell M.D., Curtis D.E., Lonie D.C., Vandermeersch T., Zurek E. and Hutchison G.R. (2012). Avogadro: An advanced semantic chemical editor, visualization, and analysis platform. *J. CHEM-INFORMATICS*, 4:17.
20. Weigend F. and Ahlrichs R. (2005). Balanced basis sets of split-valence, triple zeta valence and quadruple zeta valence quality for H to Rn: design and assessment of accuracy. *Phys. Chem. Chem. Phys.*, 7: 3297–3305.
21. Weigend F. (2006). Accurate Coulomb-fitting basis sets for H to Rn. *Phys. Chem. Chem. Phys.*, 8(9): 1057–1065.
22. Becke A.D. (1988) Density-functional exchange-energy approximation with correct asymptotic behaviour. *Phys. Rev.*, 38: 3098–3100.
23. Perdew J.P. (1986). Density-functional approximation for the correlation energy of the inhomogeneous electron gas. *Phys. Rev. B*, 34: 8822–8824.
24. Tsipis A.C. (2014) DFT flavor of coordination chemistry. *Coord. Chem. Rev.*, 272, 1–29.
25. Brandenburg J.G., Bannwarth C., Hansen A., and Grimme S. (2008) B97-3c: A revised low-cost variant of the B97-D density functional method. *J. Chem. Phys.*, 148: 064104-13.
26. Neese F. (2003). An improvement of the resolution of the identity approximation for the calculation of the coulomb matrix. *J. Comput. Chem.*, 24:1740–1747.
27. Grimme S., Antony J., Ehrlich S. and Krieg H. (2010). A consistent and accurate ab initio parametrization of density functional dispersion correction (DFT-D) for the 94 elements H–Pu. *J. Chem. Phys.*, 132: 154104.
28. Grimme S., Ehrlich S. and Goerigk L. (2011). Effect of the damping function in dispersion corrected density functional theory. *J. Comput. Chem.*, 32: 1456–1465.
29. Yan Z. and Truhlar D.G. (2008). The M06 suite of density functionals for main group thermochemistry, thermochemical kinetics, non-covalent interactions, excited states, and transition elements: Two new functionals and systematic testing of four M06-class functionals and 12 other functional. *Theor. Chem. Acc.*, 120: 215–241.
30. Neese F., Wennmohs F., Hansen A. and Becker U. (2009) Efficient, approximate and parallel Hartree–Fock and hybrid DFT calculations. A ‘chain-of-spheres’ algorithm for the Hartree–Fock exchange. *Chem. Phys.*, 356: 98–109.
31. Zhurko G.A., Chemcraft-graphical program for visualization of quantum chemistry computations, <https://chemcraftprog.com>.
32. Allen F.H., Kennard O., Watson D.G., Brammer L., Orpen, A.G. and Taylor R. (1987). Tables of bond lengths determined by X-ray and neutron diffraction, Part 1. Bond lengths in organic compounds. *J. Chem. Soc., Perkin Trans.*, 2: S1–S19.
33. Orpen A.G., Brammer L., Allen F.H., Kennard O., Watson D.G. and Taylor R (1989) Tables of bond lengths determined by X-ray and neutron diffraction. Part 2. Organometallic compounds and coordination complexes of the d- and f-block metals. *J. Chem. Soc., Dalton Trans.*, S1–S83.
34. Parr R.G. and Yang W. (1984) Density functional approach to the frontier-electron theory of chemical reactivity. *J. Am. Chem. Soc.*, 106: 4049–4050.
35. Yang W. and Mortier W.J. (1986). The use of global and local molecular parameters for the analysis of the gas-phase basicity of amines. *J. Am. Chem. Soc.*, 108:5708–5711.

Citation: Julius Numbonui Ghogomu and Fitzgerald Kogge Bine. (2020). Coordination Pattern of Two Imidazole-Chalcone Hybrid Ligands and Reactivity Analysis of Their Transition Metal (II) Complexes by Density Functional Theory. *Archives of Chemistry and Chemical Engineering* 2(1).

36. Morell C., Grand A., Gutiérrez-Oliva S. and Toro-Labbé A. (2006). Using the reactivity-selectivity descriptor $\Delta f(r)$ in organic chemistry. In: Toro-Labbé A (ed) Theoretical aspects of chemical reactivity. Elsevier, Amsterdam, 101-117.
37. Pérez P., Domingo L.R., Duque-Noreña M. and Chamorro E. (2009). A condensed-to-atom nucleophilicity index. An application to the director effects on the electrophilic aromatic substitutions. *J. Mol. Struct-THEOCHEM.*, 895: 86-91.
38. Domingo L.R., Chamorro E. and Pérez P. (2008). Understanding the reactivity of captodative ethylenes in polarcycloaddition reactions: A theoretical study. *J. Org. Chem.*, 73, 4615-4624, 2008.
39. Domingo L.R., Ríos-Gutiérrez M. and Pérez P. (2016). Applications of the Conceptual Density Functional Theory Indices to Organic Chemistry Reactivity. *Molecules*, 21, 748.
40. Bine F.K., Nkungli N.K., Numbonui T.S., and Ghogomu J.N. (2018). Structural Properties and Reactive Site Selectivity of Some Transition Metal Complexes of 2,2(1E,1E)-(ethane-1,2-diylbis (azan-1-yl-1-ylidene)) bis (phenylmethan-1-yl-1-ylidene) dibenzoic Acid: DFT, Conceptual DFT, QTAIM, and MEP Studies. *Bioinorg. Chem. Appl.*, 2018:1-11.
41. Tian L. and Feiwu C. (2012). Multiwfn: A Multifunctional Wavefunction Analyzer. *J. Comput. Chem.*, 33: 580-592.
42. Nkungli N.K., and Ghogomu J.N. (2017). Theoretical analysis of the binding of iron (III) protoporphyrin IX to 4 methoxyacetophenone thiosemicarbazone via DFT-D3, MEP, QTAIM, NCI, ELF, and LOL studies. *J. Mol. Model.*, vol. 23:200, 1-20.
43. Niepötter B., Herbst-Irmer R., Kratzert D., Samuel P.P., Mondal K.C., Roesky H.W., Jerabek P., Frenking G., and Stalke D. (2014). Experimental Charge Density Study of a Silylone. *Angew. Chem. Int. ed.*, 53:2766-2770.
44. Popelier P.L.A., (1998). Characterization of a dihydrogen bond on the basis of the electron density. *J. Phys. Chem. A*, 102: 1873-1880.
45. Espinosa E., Molins E. and Lecomte C. (1998). Hydrogen Bond Strength Revealed by Topological Analyses of Experimentally Observed Electron Densities. *Chem. Phys. Lett.*, 285(3-4): 170-173.
46. Lefebvre C., Rubez G., Khartabil H., Boisson, J., Contreras-Garcia J. and Hénon E. (2017). Accurately extracting the signature of intermolecular interactions present in the NCI plot of the reduced density gradient versus electron density. *Phys. Chem. Chem. Phys.*, 19: 17928-17936.
47. Contreras-García J., Boto R., Izquierdo-Ruiz F., Reva I., Woller T., et al. (2016). A benchmark for the non-covalent interaction (NCI) index or... is it really all in the geometry. *Theor. Chem. Acc*, 135: 242.
48. Humphrey W., Dalke A. and Schulten K. (1996). VMD-Visual Molecular Dynamics. *J. Mol. Graph.*, 14(1): 33-38.
49. Weiner P.K., Langridge R., Blaney J.M., Schaefer R., and Kollman P.A. (1982). Electrostatic potential molecular surfaces. *Proc. Natl. Acad. Sci.*, 79: 3754-3758.

Benefits of Publishing with EScientific Publishers:

- ❖ Swift Peer Review
- ❖ Freely accessible online immediately upon publication
- ❖ Global archiving of articles
- ❖ Authors Retain Copyrights
- ❖ Visibility through different online platforms

Submit your Paper at:

<https://escientificpublishers.com/submission>